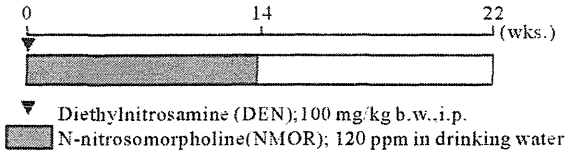

Figure 1. Protocol for an *in vivo* highly metastatic rat HCC model We had established an *in vivo* lung metastasis model of HCC induced by two hepato-carcinogens, DEN and 120 ppm NMOR. This model allows us to apply chemical substance in the intervening period to investigate modifying factors, particularly those leading to inhibition of lung metastasis formation. We attempted to establish an animal model with a simple experimental protocol and an appropriate experimental duration which would facilitate further study of the mechanisms of metastasis and antimetastatic agents.

tumors have been well characterized [10-12]. Lung metastasis by induced HCC in rats given either DEN or NMOR has been reported by Lijinsky *et al.* [13,14]. In our previous study, treatment with NMOR alone or with DEN followed by 8-weeks NMOR resulted HCC induction (**Figure 2(a)**) with only few lung metastases (**Figure 2(b)**) [9]. In contrast, DEN followed by 16 or 22-weeks NMOR treatment was associated HCC (**Figure 2(c)**) with higher frequencies of lung metastases (**Figure 2(d)**), with a duration dependence of NMOR treatment [9]. Histologically, we observed not only large metastatic nodules, but also extravasation in the lung at week 22. These findings suggest that a multi step process of metastasis (including invasion, transport, arrest, adherence, extravasation, and tumor cell proliferation) proceeded between weeks 16 and 22. Therefore, using this model, chemical substances could be applied in the intervening period to investigate modifying factors, particularly those leading to inhibition of lung metastasis formation.

Change in the expression of cadherin, a major adhesion molecule of epithelia [15-17], has been implicated in carcinogenesis because loss is frequent in human and murine high grade epithelial cancers [18-20]. In the previous study, we found that pan-cadherin expression to be decreased in the order of adenoma, HCC and advanced HCC. The quantitative difference of cadherin expression was observed between the HCC with metastasis and that without metastasis. These results suggest that down-regulation of cadherin expression may occur as an early event of carcinogenesis with decrease with in line with hyperplasia, adenoma and HCC.

Detection of circulating tumor cells in the blood may give us the evidence that tumor cells had already entered in the circulation before microscopic metastasis lesions were detected, and circulating tumor cells were also assessed in relation to HCC development and lung metastasis formation [21]. For detection of circulating

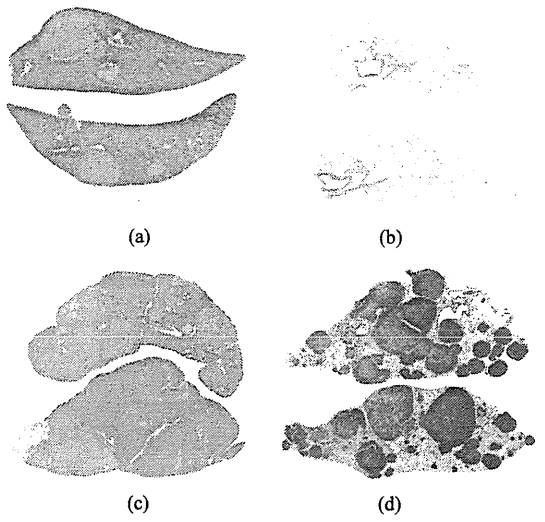

Figure 2. HCC and lung metastasis formation (a) Treatment with NMOR alone or with DEN followed by 8-weeks NMOR resulted HCC induction in week14; (b) In week 14, we observed only few lung metastases; (c) DEN followed by 14-weeks NMOR treatment induced multiple HCC; (d) We observed not only large metastatic nodules, but also extravasation in the lung at week 22.

tumor cells, RT-PCR has been utilized [22-24], and we found CK-8 expression have been demonstrated to be positive in blood. Through the travel in the circulation, only a small percentage of tumor cells (<0.01%) released from a primary tumor survive and arrest in the capillary beds of distant organs producing a successful metastasis [25]. Survival in the circulation appears to be responsible for this inefficiency due to immune factors in the blood, and this response may be the reason why tumor cells are circulating in the blood while no microscopic metastasis was found.

3. Suppression of Lung Metastasis by Aspirin but Not Indomethacin in an *in Vivo* Model of Chemically-Induced HCC

Because the metastatic cascade is a continuous process which begins with proliferation of the primary tumor and ends with proliferation of the metastatic foci [26], we hypothesized interference with cell proliferation might prevent metastasis formation. Nonsteroidal anti-inflammatory drugs (NSAIDs) such as aspirin (ASP) and indomethacin (IM) are well known as potential chemopreventive agents through their modulation of levels of prostaglandins, PGE2, and cyclooxygenase (COX) in the colon and also other organs [27,28].

We have demonstrated that ASP but not IM significantly reduced the severity of lung metastasis, but not the average number. This indicates that the effect of ASP

was marginal [29]. We also demonstrated that only ASP suppressed lung metastasis formation although ASP and IM exerted inhibitory effects on cell proliferation of HCCs [29]. Thus, it is suggested that inhibition of cell proliferation per se may not be involved in the mechanism of inhibition of lung metastasis by ASP.

Epidemiological studies revealed that NSAIDs, such as ASP and IM, which suppress COX activity, possess considerable potential as chemopreventive agents for colorectal cancer [30,31]. Constitutive expression of COX-2 has been demonstrated to lead to phenotypic changes that alter the metastatic potential of colorectal cancer cells [32], and COX-2 inhibitor was found to exert inhibitory effects on metastasis formation of various cancer [33,34]. However, our data demonstrated that IM did not suppress lung metastasis formation in spite of down-regulation of COX-2 [29], indicating no direct involvement of this enzyme in the inhibitory effect on HCC metastasis. In addition, neither ASP nor IM exerted any apparent influence on cadherin expression within HCC [29]. Therefore, the mechanism of inhibition by ASP might be mainly in a stage of the metastatic cascade after the primary site, such as attachment to the vascular endothelium or re-invasion or re-proliferation in the lung.

The attachment of a cancer cell to the vascular endothelium is a complex phenomenon involving a number of cell adhesion molecules (CAMs). Among these latter, E-selectin, ICAM-1 and VCAM-1 are considered to play primary roles in hematogenous metastasis [35,36]. Induction of Eselectin, ICAM-1 and VCAM-1 is mediated by the transcription factor nuclear factor-kappa B (NF-κB) [37,38]. ASP has been shown to inhibit NF-κB dependent transcription [39], and these transcriptions appear not to be related to the inhibition of COX activity, since IM was ineffective [40]. In the previous study, ASP significantly suppressed the expressions of ICAM-1 and VCAM-1 [29], indicating a probable role of inhibition of attachment of tumor cells to the vascular endothelium. Therefore, a stronger inhibitor of NF-κB might be expected to have a stronger inhibitory effect on lung metastasis formation.

4. Suppression of Metastasis by Nuclear Factor KappaB Inhibitors in an *in Vivo* Lung Metastasis Model of HCC

In order to evaluate the suppressive effects of NF-κB inhibitors, we examined three examples, pentoxifylline (PTX) [41], Nacetyl-L-cysteine (NAC) [42], and ASP [39], in our *in vivo* lung metastasis model. PTX, widely used as a hemorheological agent in the treatment of peripheral vascular disease, was earlier shown to suppress lung metastasis formation by B16F10 melanoma [43] and NAC inhibits VEGF production in human melanoma cell lines [44], invasion of endothelial cells [45], and invasion of human bladder cancer cells through the suppression of MMP-9 [46]. ASP has been demonstrated to inhibit angiogenesis [47] and HGF- induced invasiveness of HepG2 human hepatoma cells [48].

Among the NF-κB inhibitors, PTX exerted the strongest effects on lung metastasis formation and NAC had rather less influence, while ASP did not significantly reduce lung metastasis [49]. Although PTX and NAC suppressed lung metastasis, they did not improve the survival rates. This was mainly because the increase in the mortality rates owing to bleeding from primary HCC diminished the decrease that resulted from suppression of lung metastasis. Thus, the increase and decrease were not significant, and treatment with NF-κB inhibitors did not affect the incidences and multiplicities of HCCs in liver. Therefore, further studies are necessary to elucidate the reasons why PTX and NAC did not affect the survival rates.

To evaluate the degree of inhibition of NF-κB transcription, inhibitor of κB (IκB) protein levels in HCCs were evaluated by western blotting. The IκB family has been shown to control the function of NF-κB complexes [50,51], and IkB protein has been shown to activate NF-κB when it is phosphorylated or cleaved by proteasomes through a ubiquitine- dependent pathway [52,53]. We demonstrated that IκB protein expression was suppressed by test compounds in the order of PTX, NAC and ASP. Therefore, these results suggest that the mechanism of reduction of lung metastasis formation observed in this study may involve inhibition of NF-κB transcription.

The contribution of NF-κB to the process of metastasis has been explored in relation to CAMs and VEGF expression was found to be significantly suppressed by NF-κB signaling blockade [54], and promoted by coactivation of NF-κB [55]. PTX significantly suppressed expression of VEGF-A splicing variants with heparin-, heparin-sulfate-, and extracellular matrix-binding domains. These results suggest that the mechanism of the suppression of lung metastasis by PTX involves suppression of VEGF-A with heparin-binding domains. On the other hand, NAC, which had less influence on lung metastasis formation than PTX, suppressed VEGF-A variants with and without the heparin-binding domain. Therefore, whether NF-κB controls only VEGF-A with heparin-binding domains remains to be elucidated.

5. Conclusions

Our rat model presented here provides an excellent tool for rapid induction of metastatic HCC. To our knowledge, this is the first model to reflect the natural course

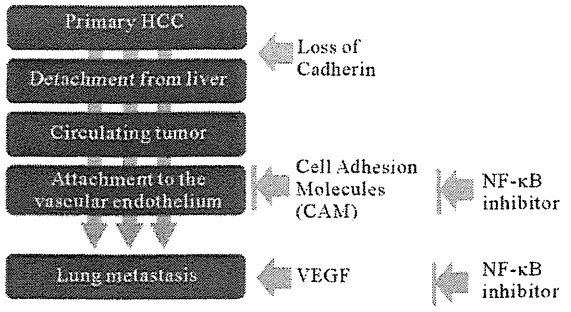

Figure 3. A multi step process of metastasis and therapeutic targets of NF-κB inhibitors A multi step process of metastasis (including invasion, transport, arrest, adherence, extravasation, and tumor cell proliferation) proceeded between weeks 16 and 22. Therefore, using this model, chemical substances could be applied in the intervening period to investigate modifying factors, particularly those leading to inhibition of lung metastasis formation. NF-κB inhibitors have the potential to inhibit lung metastasis of rat HCCs *in vivo*, with PTX being the most promising candidate. They may interfere with attachment of tumor cells to the vascular endothelium at metastatic sites, and decrease of VEGF-A188 may play an important role.

of malignant tumors which metastasize to lung, and this model should be applicable not only for the elucidation of mechanisms underlying metastasis, but also to test anti-metastatic agents.

ASP, but not IM, has the potential to inhibit lung metastasis by rat HCC *in vivo*, the mechanism apparently involving neither inhibition of cell proliferation nor detachment from primary tumors. Inhibition of attachment to the vascular endothelium in the lung is more likely to be the mechanism responsible for the suppression of lung metastasis formation by ASP. NF-κB inhibitors have the potential to inhibit lung metastasis of rat HCCs *in vivo*, with PTX being the most promising candidate. They may interfere with attachment of tumor cells to the vascular endothelium at metastatic sites, and decrease of VEGF-A188 may play an important role (**Figure 3**).

This *in vivo* model for induction of rat highly metastatic hepatocellular carcinomas is clearly a useful tool for the assessment of the efficacy of therapeutic treatments for metastasis formation and for analysis of individual steps in the metastatic process.

6. Acknowledgements

The author thanks Dr. Rakesh K. Singh (Department of Pathology and Microbiology, University of Nebraska Medical Center) for expert suggestions and comments. This work was supported in part by a research grant from Scientific Support Programs for Cancer Research Grant-in-Aid for Scientific Research on Innovative Areas Ministry of Education, Culture, Sports, Science and Technology, and a grant-in-aid for Scientific Research (C) from the Japan Society for Promotion of Science.

REFERENCES

[1] A. Jemal, F. Bray, M.M. Center, J. Ferlay, E. Ward and D. Forman, "Global Cancer Statistics," *CA: A Cancer Journal for Clinicians*, Vol. 61, No. 2, 2011, pp. 69-90. doi:caac.20107[pii]10.3322/caac.20107

[2] D. B. Walsh, S. Downing, R. Nauta and M. N. Gomes, "Metastatic Cancer. A Relative Contraindication to Vena cava Filter Placement," *Cancer*, Vol. 59, No. 1, 1987, pp. 161-163. doi:10.1002/1097-0142(19870101)59:1<161::AID-CNCR2820590131>3.0.CO;2-A

[3] I. J. Fidler, "Critical Factors in the Biology of Human Cancer Metastasis: Twenty-Eighth G.H.A. Clowes Memorial Award Lecture," *Cancer Research*, Vol. 50, No. 19, 1990, pp. 6130-6138.

[4] J. E. Talmadge and I. J. Fidler, "AACR Centennial Series: The Biology of Cancer Metastasis: Historical Perspective," *Cancer Research*, Vol. 70, No. 14, 2010, pp. 5649-5669. doi:10.1158/0008-5472.CAN-10-1040

[5] K. Morikawa, S. M. Walker, J. M. Jessup and I. J. Fidler, "*In Vivo* Selection of Highly Metastatic Cells from Surgical Specimens of Different Primary Human Colon Carcinomas Implanted into Nude Mice," *Cancer Research*, Vol. 48, 1988, pp. 1943-1948.

[6] X. B. Li, J. Hamada, N. Takeichi, M. Hosokawa and H. Kobayashi, "Timing of UFT Administration Combined with Surgical Operation in Pulmonary Metastasis of Rat Mammary Carcinoma," *Japanese Journal of Cancer and Chemotherapy*, Vol. 16, No. 7, 1989, pp. 2381-2385.

[7] I. J. Fidler and M. L. Kripke, "Metastasis Results from Preexisting Variant Cells within a Malignant Tumor," *Science*, Vol. 197, No. 4306, 1977, pp. 893-895. doi:10.1126/science.887927

[8] T. Masui, H. Nakanishi, K. Inada, T. Imai, Y. Mizoguchi, H. Yada, M. Futakuchi, T. Shirai and M. Tatematsu, "Highly Metastatic Hepatocellular Carcinomas Induced in Male F344 Rats Treated with N-Nitrosomorpholine in Combination with Other Hepatocarcinogens Show a High Incidence of p53 Gene Mutations Along with Altered mRNA Expression of Tumor-Related Genes," *Cancer Letters*, Vol. 112, No. 1, 1997, pp. 33-45. doi:10.1016/S0304-3835(96)04543-0

[9] M. Futakuchi, M. Hirose, T. Ogiso, K. Kato, M. Sano, K. Ogawa and T. Shirai, "Establishment of an *in Vivo* Highly Metastatic Rat Hepatocellular Carcinoma Model," *Japanese Journal of Cancer and Chemotherapy*, Vol. 90, No. 11, 1999, pp. 1196-1202. doi:10.1111/j.1349-7006.1999.tb00695.x

[10] H. Enzmann, H. Zerban, S. A. Kopp, E. Loser and P. Bannach, "Effects of Low Doses of N-Nitrosomorpholine on the Development of Early Stages of Hepatocarcinogenesis," *Carcinogenesis*, Vol. 16, No. 7, 1995, pp. 1513-1518. doi:10.1093/carcin/16.7.1513

[11] M. Volm, H. Zerban, J. Mattern and T. Efferth, "Overexpression of P-Glycoprotein in Rat Hepatocellular Carci-

nomas Induced with N-Nitrosomorpholine," *Carcinogenesis*, Vol. 11, No. 1, 1990, pp. 169-172. doi:10.1093/carcin/11.1.169

[12] E. Weber and P. Bannasch, "Dose and Time Dependence of the Cellular Phenotype in Rat Hepatic Preneoplasia and Neoplasia Induced by Continuous Oral Exposure to N-Nitrosomorpholine," *Carcinogenesis*, Vol. 15, No. 6, 1994, pp. 1235-1242. doi:10.1093/carcin/15.6.1235

[13] W. Lijinsky, "Metastasizing Tumors in Rats Treated with Alkylating Carcinogens," *Carcinogenesis*, Vol. 16, No. 4, 1995, pp. 675-681. doi:10.1093/carcin/16.4.675

[14] W. Lijinsky, R. M. Kovatch, C. W. Riggs and P. T. Walters, "Dose-Response Study with N-Nitrosomorpholine in Drinking Water of F-344 Rats," *Cancer Research*, Vol. 48, No. 8, 1988, pp. 2089-2095.

[15] M. Takeichi, "Cadherin Cell Adhesion Receptors as a Morphogenetic Regulator," *Science*, Vol. 251, No. 5000, 1991, pp. 1451-1455. doi:10.1126/science.2006419

[16] M. Takeichi, M. Watabe, S. Shibamoto and F. Ito, "Cadherin-Dependent Organization and Disorganization of Epithelial Architecture," *Princess Takamatsu Symposia*, Vol. 24, 1994, pp. 28-37.

[17] M. Takeichi, "Morphogenetic Roles of Classic Cadherins," *Current Opinion in Cell Biology*, Vol. 7, 5, 1995, pp. 619-627. doi:10.1016/0955-0674(95)80102-2

[18] R. Umbas, J. A. Schalken, T. W. Aalders, B. S. Carter, H. F. Karthaus, H. E. Schaafsma, F. M. Debruyne and W. B. Isaacs, "Expression of the Cellular Adhesion Molecule E-Cadherin Is Reduced or Absent in High-Grade Prostate Cancer," *Cancer Research*, Vol. 52, No. 18, 1992, pp. 5104-5109.

[19] P. Navarro, M. Gomez, A. Pizarro, C. Gamallo, M. Quintanilla and A. Cano, "A Role for the E-Cadherin cell-Cell Adhesion Molecule during Tumor Progression of Mouse Epidermal Carcinogenesis," *The Journal of Cell Biology*, Vol. 115, No. 2, 1991, pp. 517-533. doi:10.1083/jcb.115.2.517

[20] S. Wakatsuki, R. Watanabe, K. Saito, T. Saito, A. Katagiri, S. Sato and Y. Tomita, "Loss of Human E-Cadherin (ECD) Correlated with Invasiveness of Transitional Cell Cancer in the Renal Pelvis, Ureter and Urinary Bladder," *Cancer Letters*, Vol. 103, No. 1, 1996, pp. 11-17. doi:10.1016/0304-3835(96)04194-8

[21] H. Yoshino, M. Futakuchi, Y. M. Cho, K. Ogawa, F. Takeshita, N. Imai, S. Tamano and T. Shirai, "Modification of an *in Vivo* Lung Metastasis Model of Hepatocellular Carcinoma by Low Dose N-Nitrosomorpholine and Diethylnitrosamine," *Clinical and Experimental Metastasis*, Vol. 22, No. 5, 2005, pp. 441-447. doi:10.1007/s10585-005-2807-9

[22] S. Ito, H. Nakanishi, T. Hirai, T. Kato, Y. Kodera, Z. Feng, Y. Kasai, K. Ito, S. Akiyama, A. Nakao and M. Tatematsu, "Quantitative Detection of CEA Expressing Free Tumor Cells in the Peripheral Blood of Colorectal Cancer Patients during Surgery with Real-Time RT-PCR on a LightCycler," *Cancer Letters*, Vol. 183, No. 2, 2002, pp. 195-203. doi:10.1016/S0304-3835(02)00157-X

[23] M. Matsumura, Y. Niwa, Y. Hikiba, K. Okano, N. Kato, S. Shiina, Y. Shiratori and M. Omata, "Sensitive Assay for Detection of Hepatocellular Carcinoma Associated Gene Transcription (Alpha-Fetoprotein mRNA) in Blood," *Biochemical and Biophysical Research Communications*, Vol. 207, No. 2, 1995, pp. 813-818. doi:10.1006/bbrc.1995.1259

[24] Y. Miyajima, K. Horibe, M. Fukuda, K. Matsumoto, S. Numata, H. Mori and K. Kato, "Sequential Detection of Tumor Cells in the Peripheral Blood and Bone Marrow of Patients with Stage IV Neuroblastoma by the Reverse Transcription-Polymerase Chain Reaction for Tyrosine Hydroxylase mRNA," *Cancer*, Vol. 77, No. 6, 1996, pp. 1214-1219. doi:10.1002/(SICI)1097-0142(19960315)77:6<1214::AID-CNCR31>3.0.CO;2-2

[25] K. J. Luzzi, I. C. MacDonald, E. E. Schmidt, N. Kerkvliet, V. L. Morris, A. F. Chambers and A. C. Groom, "Multistep Nature of Metastatic Inefficiency: Dormancy of Solitary Cells after Successful Extravasation and Limited Survival of Early Micrometastases," *American Journal of Pathology*, Vol. 153, No. 3, 1998, pp. 865-873. doi:10.1016/S0002-9440(10)65628-3

[26] I. J. Fidler, "The Pathogenesis of Cancer Metastasis: The 'Seed and Soil' Hypothesis Revisited," *Nature Reviews Cancer*, Vol. 3, No. 6, 2003, pp. 453-458. doi:10.1038/nrc1098

[27] A. T. Chan and N. R. Cook, "Are We Ready to Recommend Aspirin for Cancer Prevention?" *Lancet*, Vol. 379, No. 9826, 2012, pp. 1569-1571. doi:10.1016/S0140-6736(11)61654-1

[28] T. F. Imperiale, "Aspirin and the Prevention of Colorectal Cancer," *The New England Journal of Medicine*, Vol. 348, 2003, pp. 879-880. doi:10.1056/NEJMp030005

[29] M. Futakuchi, K. Ogawa, M. Sano, S. Tamano, F. Takeshita and T. Shirai, "Suppression of Lung Metastasis by Aspirin but Not Indomethacin in an *in Vivo* Model of Chemically Induced Hepatocellular Carcinoma," *Japanese Journal of Cancer Research*, Vol. 93, No. 10, 2002, pp. 1175-1181. doi:10.1111/j.1349-7006.2002.tb01220.x

[30] N. Murashige, M. Kami and M. Ikeda, "Aspirin, COX-2, and the Risk of Colorectal Cancer," *The New England Journal of Medicine*, Vol. 357, 2007, pp. 824-825; Author Reply pp. 824-825. doi:10.1056/NEJMc071797

[31] Y. J. Zhang, Y. J. Bao, Q. Dai, W. Y. Yang, P. Cheng, L. M. Zhu, B. J. Wang and F. H. Jiang, "mTOR Signaling Is Involved in Indomethacin and Nimesulide Suppression of Colorectal Cancer Cell Growth via a COX-2 Independent Pathway," *Annals of Surgical Oncology*, Vol. 18, No. 2, 2011, pp. 580-588. doi:10.1245/s10434-010-1268-9

[32] M. Tsujii, S. Kawano and R. N. DuBois, "Cyclooxygenase-2 Expression in Human Colon Cancer Cells Increases Metastatic Potential," *Proceedings of the National Academy of Sciences of the United States*, Vol. 94, No. 7, 1997, pp. 3336-3340. doi:10.1073/pnas.94.7.3336

[33] M. Farooqui, Y. Li, T. Rogers, T. Poonawala, R.J. Griffin, C.W. Song, K. Gupta, "COX-2 Inhibitor Celecoxib Prevents Chronic Morphine-Induced Promotion of Angiogenesis, Tumour Growth, Metastasis and Mortality, with-

out Compromising Analgesia," *British Journal of Cancer*, Vol. 97, No. 11, 2007, pp. 1523-1531. doi:10.1038/sj.bjc.6604057

[34] B. Singh, J. A. Berry, A. Shoher, G. D. Ayers, C. Wei and A. Lucci, "COX-2 Involvement in Breast Cancer Metastasis to Bone," *Oncogene*, Vol. 26, No. 26, 2007, pp. 3789-3796. doi:10.1038/sj.onc.1210154

[35] Q. Chen and J. Massague, "Molecular Pathways: Vcam-1 as a Potential Therapeutic Target in Metastasis," *Clinical Cancer Research*, Vol. 18, No. 20, 2012, pp. 5520-5525. doi:10.1158/1078-0432.CCR-11-2904

[36] J. P. Johnson, B. G. Stade, B. Holzmann, W. Schwable and G. Riethmuller, "De Novo Expression of Intercellular-Adhesion Molecule 1 in Melanoma Correlates with Increased Risk of Metastasis," *Proceedings of the National Academy of Sciences of the United States A*, Vol. 86, No. 2, 1989, pp. 641-644. doi:10.1073/pnas.86.2.641

[37] C. Lawson, M. Ainsworth, M. Yacoub and M. Rose, "Ligation of ICAM-1 on Endothelial Cells Leads to Expression of VCAM-1 via a Nuclear Factor-KappaB-Independent Mechanism," *The Journal of Immunology*, Vol. 162, No. 5, 1999, pp. 2990-2996.

[38] D. Zapolska-Downar and M. Naruszewicz, "Propionate Reduces the Cytokine-Induced VCAM-1 and ICAM-1 Expression by Inhibiting Nuclear Factor-Kappa B (NF-KappaB) Activation," *Journal of physiology and pharmacology*, Vol. 60, No. 2, 2009, pp. 123-131.

[39] E. Kopp and S. Ghosh, "Inhibition of NF-Kappa B by Sodium Salicylate and Aspirin," *Science*, Vol. 265, No. 5174, 1994, pp. 956-959. doi:10.1126/science.8052854

[40] C. Weber, W. Erl, A. Pietsch and P. C. Weber, "Aspirin Inhibits Nuclear Factor-Kappa B Mobilization and Monocyte Adhesion in Stimulated Human Endothelial Cells," *Circulation*, Vol. 91, No. 7, 1995, pp. 1914-1917. doi:10.1161/01.CIR.91.7.1914

[41] D. K. Biswas, C. M. Ahlers, B. J. Dezube and A. B. Pardee, "Pentoxifylline and Other Protein Kinase C Inhibitors Down-Regulate HIV-LTR NF-Kappa B Induced Gene Expression," *Molecular Medicine*, Vol. 1, No. 1, 1994, pp. 31-43.

[42] M. Roederer, P. A. Raju, F. J. Staal and L. A. Herzenberg, "N-Acetylcysteine Inhibits Latent HIV Expression in Chronically Infected Cells," *AIDS Research and Human Retroviruses*, Vol. 7, No. 6, 1991, pp. 563-567. doi:10.1089/aid.1991.7.563

[43] V. P. Sant, M. S. Nagarsenker, S. G. Rao and R. P. Gude, "Enhancement of Anti-Metastatic Activity of Pentoxifylline by Encapsulation in Conventional Liposomes and Sterically Stabilized Liposomes in Murine Experimental B16F10 Melanoma Model," *Journal of Pharmacy and Pharmacology*, Vol. 52, No. 12, 2000, pp. 1461-1466. doi:10.1211/0022357001777667

[44] P. Redondo, E. Bandres, T. Solano, I. Okroujnov and J. Garcia-Foncillas, "Vascular Endothelial Growth Factor (VEGF) and Melanoma. N-Acetylcysteine Downregulates VEGF Production *in Vitro*," *Cytokine*, Vol. 12, No. 4, 2000, pp. 374-378. doi:10.1006/cyto.1999.0566

[45] T. Cai, G. Fassina, M. Morini, M. G. Aluigi, L. Masiello, G. Fontanini, F. D'Agostini, S. De Flora, D. M. Noonan and A. Albini, "N-Acetylcysteine Inhibits Endothelial Cell Invasion and Angiogenesis," *Laboratory Investigation*, Vol. 79, No. 9, 1999, pp. 1151-1159.

[46] S. Kawakami, Y. Kageyama, Y. Fujii, K. Kihara and H. Oshima, "Inhibitory Effect of N-Acetylcysteine on Invasion and MMP-9 Production of T24 Human Bladder Cancer cells," *Anticancer Research*, Vol. 21, No. 1A, 2001, pp. 213-219.

[47] M. K. Jones, H. Wang, B. M. Peskar, E. Levin, R. M. Itani, I. J. Sarfeh and A. S. Tarnawski, "Inhibition of Angiogenesis by Nonsteroidal Anti-Inflammatory Drugs: Insight into Mechanisms and Implications for Cancer Growth and Ulcer Healing," *Nature Medicine*, Vol. 5, No. 12, 1999, pp. 1418-1423. doi:10.1038/70995

[48] S. Abiru, K. Nakao, T. Ichikawa, K. Migita, M. Shigeno, M. Sakamoto, H. Ishikawa, K. Hamasaki, K. Nakata and K. Eguchi, "Aspirin and NS-398 Inhibit Hepatocyte Growth Factor-Induced Invasiveness of Human Hepatoma Cells," *Hepatology*, Vol. 35, No. 5, 2002, pp. 1117-1124. doi:10.1053/jhep.2002.32676

[49] M. Futakuchi, K. Ogawa, S. Tamano, S. Takahashi and T. Shirai, "Suppression of Metastasis by Nuclear Factor Kappab Inhibitors in an *in Vivo* Lung Metastasis Model of Chemically Induced Hepatocellular Carcinoma," *Cancer Science*, Vol. 95, No. 1, 2004, pp. 18-24. doi:10.1111/j.1349-7006.2004.tb03165.x

[50] V. Blank, P. Kourilsky and A. Israel, "NF-Kappa B and Related Proteins: Rel/Dorsal Homologies Meet Ankyrin-Like Repeats," *Trends in Biochemical Sciences*, Vol. 17, No. 4, 1992, pp. 135-140. doi:10.1016/0968-0004(92)90321-Y

[51] G. P. Nolan and D. Baltimore, "The Inhibitory Ankyrin and Activator Rel Proteins," *Current Opinion in Genetics & Development*, Vol. 2, No. 2, 1992, pp. 211-220. doi:10.1016/S0959-437X(05)80276-X

[52] G. Dong, Z. Chen, T. Kato and C. Van Waes, "The Host Environment Promotes the Constitutive Activation of Nuclear Factor-KappaB and Proinflammatory Cytokine Expression during Metastatic Tumor Progression of Murine Squamous Cell Carcinoma," *Cancer Research*, Vol. 59, 14, 1999, pp. 3495-3504.

[53] L. Lin, G. N. DeMartino and W. C. Greene, "Cotranslational Biogenesis of NF-KappaB p50 by the 26S Proteasome," *Cell*, Vol. 92, No. 6, 1998, pp. 819-828. doi:10.1016/S0092-8674(00)81409-9

[54] S. Huang, C. A. Pettaway, H. Uehara, C. D. Bucana and I. J. Fidler, "Blockade of NF-KappaB Activity in Human Prostate Cancer Cells Is Associated with Suppression of Angiogenesis, Invasion, and Metastasis," *Oncogene*, Vol. 20, No. 31, 2001, v4188-4197. doi:10.1038/sj.onc.1204535

[55] H. M. Ko, K. H. Seo, S. J. Han, K. Y. Ahn, I. H. Choi, G. Y. Koh, H. K. Lee, M. S. Ra and S. Y. Im, "Nuclear Factor KappaB Dependency of Platelet-Activating Factor-Induced Angiogenesis," *Cancer Research*, Vol. 62, No. 6, 2002, pp. 1809-1814.

Promotive effects of cell proliferation and chromosomal instability induced by tribbles-related protein 3 in mouse mammary tumor cells

YUTO SAKAI[1,2], KATSUMI FUKAMACHI[1], MITSURU FUTAKUCHI[1], HIDETOSHI HAYASHI[2] and MASUMI SUZUI[1]

[1]Department of Molecular Toxicology, Nagoya City University Graduate School of Medical Sciences and Medical School, 1 Kawasumi, Mizuho-cho, Mizuho-ku, Nagoya 467-8601; [2]Department of Drug Metabolism and Disposition, Nagoya City University Graduate School of Pharmaceutical Sciences, 3-1 Tanabe-dori, Mizuho-ku, Nagoya 467-8603, Japan

Received January 23, 2013; Accepted March 28, 2013

DOI: 10.3892/or.2013.2441

Abstract. Tribbles-related protein 3 (TRB3) has been shown to be a crucial modulator of tumorigenesis. However, the precise role and the functional morphology of TRB3 are not clearly understood. To elucidate these enigmas we established the cell line, M2TRB3, by introducing the human TRB3 gene and protein in Cl66M2 (M2) mouse mammary tumor cells. This cell line stably expressed the TRB3 gene and protein. After 72 h of cell culture, there was a 34% increase in the growth of M2TRB3 cells compared to the control M2 mock cells. The mean volume of the tumors originating from the M2TRB3 cells was significantly increased by 38% when compared to the mean volume of the M2 mock tumors, and the proliferating cell nuclear antigen (PCNA) labeling index in the M2TRB3 tumors was higher when compared to that of the M2 and M2 mock cells. In the tumor tissue samples, the mean diameter of nuclei in the M2TRB3 tumor cells (9.4±0.3 μm) showed a significant increase compared to that of the M2 mock tumor cells (7.0±0.2 μm). M2TRB3 cells also showed a marked increase in the population of tetraploid or octaploid nuclei compared to M2 mock cells bearing mainly either diploid or tetraploid nuclei. Western blot analysis revealed the overexpression of cyclin B1 and cyclin D1 in M2TRB3 cells when compared to that in the M2 mock cells. These novel findings provide further evidence that TRB3 promotes cell proliferation and chromosomal instability by causing polyploidization during development.

Correspondence to: Dr Masumi Suzui, Department of Molecular Toxicology, Nagoya City University Graduate School of Medical Sciences and Medical School, 1 Kawasumi, Mizuho-cho, Mizuho-ku, Nagoya 467-8601, Japan
E-mail: suzui@med.nagoya-cu.ac.jp

Key words: tribbles-related protein 3, cell proliferation, ploidy, tumor xenograft

Introduction

Tribbles-related protein 3 (TRB3, also known as NIPK, SKIP3) is a mammalian homologue of the *Drosophila Tribbles* gene, and this gene has been identified as an inhibitor of mitosis that regulates cell proliferation, migration and morphogenesis during development (1-3). Among tribbles homologues TRB1, TRB2 and TRB3, TRB3 is the most recently defined family of pseudokinases that contain a serine/threonine kinase catalytic domain but lack an ATP binding site or one of the conserved catalytic motifs essential for kinase activity (4). The interacting partners of TRB3 range from transcription factors, ubiquitin ligase, bone morphogenetic protein (BMP) type II receptor to members of the mitogen-activated protein kinase (MAPK) and phosphoinositide 3-kinase (PI3K) signaling pathways. By interacting with these proteins, it coordinates crucial cellular processes, including glucose/lipid metabolism, apoptosis, adipocyte differentiation, cell stress and regulation of collagen expression (5-9). We previously demonstrated that TRB3 is induced by C/EBP homologous protein (CHOP) and activating transcription factor 4 (ATF4) to regulate their function and endoplasmic reticulum (ER) stress-induced cell death (10) and that TRB3 also regulates the stability of cell division cycle 25A (Cdc25A), an essential activator of cyclin-dependent kinases (CDKs) (11).

Recent studies indicate that the three mammalian tribbles homologues are crucial modulators of tumorigenesis. For instance, both TRB1 and TRB2 are involved in myeloid leukemogenesis (12,13). TRB3 is highly expressed in a wide range of human carcinoma cell lines and in several types of human carcinomas (4,14). However, a precise role of TRB3 in tumorigenesis remains unknown. The aim of the present study was to examine whether the introduction of the human *TRB3* gene into mouse mammary tumor cells affects *in vitro*/*in vivo* growth and chromosomal stability during cell division of tumor cells.

Materials and methods

Cell culture. The human embryonic kidney cell line 293 purchased from the American Type Culture Collection (ATCC,

Manassas, VA, USA) and the human hepatocellular carcinoma cell line HepG2 were cultured in Dulbecco's modified Eagle's medium (DMEM; Wako Pure Chemical Industries, Ltd., Osaka, Japan) supplemented with 10% fetal bovine serum (FBS; Life Technologies, Inc., Rockville, MD, USA) in a humidified incubator with 5% CO_2 at 37°C. The murine mammary tumor cell line Cl66M2 (M2) was generously provided by Dr Rakesh K. Singh (University of Nebraska Medical Center, Omaha, NE, USA) (18) and cultured in DMEM supplemented with 5% FBS in a humidified incubator with 5% CO_2 at 37°C.

Construction of the expression vector. The TRB3 flag-tagged expression vector was constructed by ligating the full length human TRB3 cDNA into *Bam*HI and *Xho*I restriction sites of pcDNA3.1-Hygro (Life Technologies, Inc.) (9). The construct was verified by sequencing.

Preparation of a cell line that stably expresses the TRB3 gene. The expression vector pcDNA3.1-Hygro-flag-human TRB3 was transfected into Cl66M2 cells using Lipofectamine 2000 reagent (Life Technologies, Inc.). This cell line was termed M2TRB3. After transfection, the clone of the cells stably expressing M2TRB3 was selected by a limiting-dilution method in culture media supplemented with hygromycin. The cells transfected with the empty vector were also prepared as the control (M2mock). In M2TRB3 and M2mock cells, the levels of mRNA and protein expression were confirmed by reverse transcription-polymerase chain reaction (RT-PCR) and western blot assays.

In vitro cell proliferation assay. These assays were performed as described previously by us (15). Two murine mammary tumor cell lines M2TRB3 and M2mock were plated into 6-well 35-mm diameter culture plates ($1.0x10^4$ cells/well) in DMEM containing 10% FBS. Cells were starved in DMEM containing 0.5% FBS for 48 h. After starvation, the culture media were removed and cells were grown in DMEM containing 10% FBS for the indicated time course (0-72 h). The cells were washed twice with phosphate-buffered saline (PBS), harvested, resuspended in 1 ml PBS and the number of cells was determined using a hemocytometer Burker-Turk (Erma Inc., Tokyo, Japan). Each assay was repeated more than three times to confirm the results. The number of cells was plotted on a time-response curve as indicated in the figures.

Tumor xenograft assay. Male four-week-old BALB/cSlc-nu/nu mice obtained from Japan SLC, Inc. (Shizuoka Japan) were used. M2, M2TRB3 and M2mock cells ($1.0x10^6$/200 μl) were subcutaneously inoculated into the right lower flank of the mice. Tumor diameters (mm) and body weight (g) were recorded twice weekly. The tumor volume (mm^3) was calculated by the formula: Volume = L x D x H x π/6, where L is the length, D is the depth, and H is the height. At 35 days after inoculation, all mice were euthanized and complete autopsies were performed. Animal experiments were conducted in accordance to the regulations specified by the Institutional Animal Use and Care Committee of Nagoya City University.

Immunohistochemistry and measurement of proliferating cell nuclear antigen (PCNA) labeling index. These assays were performed using an established method as described previously by us (16). Paraffin sections (3-μm) were prepared to include tumors resected from the lower flank of each mouse. These sections were treated in 3% H_2O_2 for 10 min to block the endogenous peroxidase activity. For antigen retrieval, the sections were brought to boiling in 0.1 M citrate buffer, pH 6.0. Sections were incubated with a primary antibody of PCNA (1:500 dilution) (sc-56; Santa Cruz Biotechnology, Inc., Santa Cruz, CA, USA) at room temperature for 60 min. After incubation with the secondary antibody, sections were then stained using an ABC kit (Vector Laboratories, Inc., Burlingame, CA, USA) according to the manufacturer's instructions. The PCNA labeling index was determined by calculating the ratio of PCNA-positive nuclei/total number of nuclei counted. Ten high power fields (x400) per tumor were examined, and >300 cells were counted in each tumor. In M2TRB3 and M2mock tumors, the longest diameter of the nucleus was determined by image analysis using Olympus DP70 system (Olympus Corp., Tokyo, Japan). Four high power fields (x400) per tumor were examined and more than 100 nuclei were counted in each tumor.

Flow cytometric analysis. These assays were performed as previously described (16). M2TRB3 and M2mock cells ($7.5x10^4$ cells/plate) were plated onto 9-cm culture dishes in DMEM plus 10% FBS and grown to yield 50-60% confluence. To synchronize cells at the G0/G1 phase, they were starved by culturing in DMEM plus 0.5% FBS for 48 h. After starvation, cells were then growth in DMEM plus 10% FBS for 72 h. Adherent cells were washed twice with PBS, fixed with 5 ml 70% ethanol, centrifuged, resuspended in 400 μl PBS containing 2 mg/ml RNase (Nacalai Tesque, Inc., Kyoto, Japan), and stained with 400 μl of 0.1 mg/ml propidium iodide (Sigma-Aldrich, St. Louis, MO, USA) in the dark for 30 min or overnight. The cell suspension was filtered through a 60-μm nylon filter (Ikemoto Scientific Technology Co., Ltd., Tokyo). Samples of 10,000-20,000 cells were then analyzed for cell cycle phase distribution and ploidy status using a FACSCalibur™ instrument, and the data were analyzed with the CellQuest computer program (both from Becton-Dickinson, Franklin lakes, NJ, USA) as described in a previous study (16). Cells were harvested just after starvation (0 h) and 72 h after starvation as described in Table I and Fig. 5. Each assay was repeated more than three times to confirm the results.

RT-PCR assays. These assays were conducted using previously established procedures (16). Total RNA was extracted from each cell line grown in 9-cm culture dishes using Isogen (Nippon Gene, Toyama, Japan). The reaction mixture contained 4 μg of total RNA, 1 μl of 10 mM dNTP, 1 μl of random primers (both from Life Technologies, Inc.) and 7 μl of distilled water. The reaction mixture was incubated at 65°C (5 min) for denaturation, chilled on ice for 1 min and 4 μl of 5X RT buffer (Life Technologies, Inc.), 1 μl of 0.1 M dithiothreitol (DTT), 1 μl of the RNaseOut and 1 μl of Superscript® III Reverse Transcriptase (both from Life Technologies, Inc.) were added. After the addition of these reagents, the reaction mixture was incubated at 50°C (60 min) for random primer annealing and 70°C (15 min) for cDNA preparation. One microliter of the reaction mixture was then used for PCR. The primer sequences used in this study were as follows: human TRB3-specific

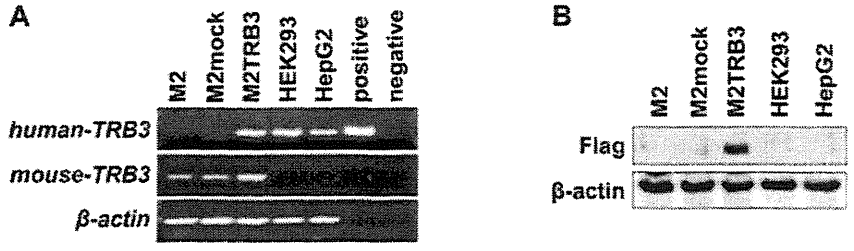

Figure 1. Expression status of exogenous human TRB3 and endogenous mouse TRB3 in the indicated cell lines. (A) Representative results of the RT-PCR analysis. The band in the positive control was derived from DNA fragments that were PCR-amplified using pcDNA3.1-Hygro-flag-human TRB3 vector as a template and the pairs of gene-specific primers listed in Materials and methods. No band was noted in the negative control since the empty vector (pcDNA3.1-Hygro) that does not carry specific sites for the primers was used as a template for PCR. Bands of β-actin were not observed in the positive and negative control samples due to the same reason as the negative control. (B) Representative results of the western blot analysis. The exogenous human TRB3 (Flag) protein was detected in the M2TRB3 cells.

primer set, hTRB3F (5'-CAAGTCGCTCTGAAGGTTCC-3') and hTRB3R (5'-CCATCCTACTCTGGCAAAGC-3'), mouse TRB3-specific primer set, mTRB3F (5'-CAAGTCGCTCT GAAGGTTCC-3') and mTRB3R (5'-CCATCCTACTC TGGCAAAGC-3'), respectively.

β-actin-specific DNA fragments from the same RNA samples were amplified and served as internal controls. Primers actinF (5'-CCGTAAAGACCTCTATGCCAACA-3') and actinR (5'-CGGACTCATCGTACTCCTGCTT-3') were used for amplification of β-actin. PCR was conducted for 26-30 cycles in an iCycler (Bio-Rad Laboratories, Inc., Hercules, CA, USA). Each amplification cycle consisted of 0.5 min at 94°C for denaturation, 0.5 min at 60°C for primer annealing, and 1 min at 72°C for extension. After PCR amplification, the DNA fragments were stained with ethidium bromide and analyzed by 2% agarose gel electrophoresis. The results were confirmed by repeating the experiments.

Western blot assays. These assays were conducted according to previously established procedures (17). The cells were lysed in radioimmunoprecipitation assay (RIPA) buffer [50 mM Tris-HCl (pH 8.0), 150 mM NaCl, 0.1% sodium dodecyl sulfate (SDS), 0.5% deoxycholate, and 1% Triton X-100]. The lysates were subjected to SDS-polyacrylamide gel electrophoresis (PAGE) (12.5%), transferred onto a polyvinylidene difluoride (PVDF) membrane (Immobilon P; Millipore Corp., Bedford, MA, USA) and probed with the antibodies. The primary antibodies used in the present study were anti-β-actin monoclonal antibody (AC-15) (Sigma-Aldrich), anti-cyclin B1 monoclonal antibody (sc-245) (Santa Cruz Biotechnology Inc.), anti-Cdc2 monoclonal antibody (sc-54), anti-Cdk2 polyclonal antibody (sc-163), anti-Cdk4 polyclonal antibody (sc-260), anti-TRB3 polyclonal antibody (sc-34211), anti-cyclin D1 monoclonal antibody (556470; Becton-Dickinson), and anti-Flag monoclonal antibody (018-22381) (Wako Pure Chemical Industries, Ltd.). The immunoreactive proteins were visualized using ImmunoStar Zeta (Wako Pure Chemical Industries, Ltd.) and light emission was quantified with Light Capture (ATTO Corp., Tokyo, Japan). Each assay was repeated more than three times to confirm the results.

Statistical analysis. Differences in the number of cells, tumor volume, PCNA labeling index, and rate of DNA ploidy between cell lines or tumor origins were analyzed by the Student's or Welch's t-test. A value of $P<0.05$ was considered to indicate a statistically significant result.

Results

TRB3 expression in the M2TRB3 cells. To examine the role of TRB3 in cell proliferation, we developed a cell line (M2TRB3) that stably expresses the human *TRB3* gene by transfecting the gene into murine mammary tumor cell line Cl66M2 (M2) (18). We also developed the control cells (M2mock) transfected with empty vector pcDNA3.1-Hygro. M2TRB3 cells expressed both human *TRB3* mRNA and mouse *TRB3* mRNA (Fig. 1A). Human embryonic kidney cell line HEK293 and human hepatoma cell line HepG2 also expressed human *TRB3* mRNA. There was no mRNA expression of human TRB3 in the M2 and M2mock cells. Human TRB3 DNA was PCR-amplified from pcDNA3.1-Hygro-flag-human TRB3 vector and the band was present in the positive lane in Fig. 1A. Expression of the exogenous TRB3 protein (Flag) was present in the M2TRB3 cells. No expression was noted in the protein samples derived from M2, M2mock, HEK293 and HepG2 cells (Fig. 1B). The M2TRB3 and M2mock cells were used for cell proliferation assays.

TRB3 gene enhances cell proliferation and tumor volume. To examine the tumorigenic activity of the TRB3 gene, we investigated its effects on cell and tumor growth using M2TRB3 and M2mock cells. The number of M2TRB3 cells significantly increased compared to M2mock cells at the 48 and 72 h time points ($P<0.01$ and 0.05, respectively) (Fig. 2A). At 72 h, a 34% increase was noted in the number of M2TRB3 cells compared to that of the M2mock cells. To examine the extent of M2TRB3 cell growth when these cells were implanted into the subcutaneous tissue of mice, we used the xenograft mouse model as described in Materials and methods. Twice a week observation was carried out with all mice throughout the experiment. Tumor growth was monitored with the naked eye from day 7 to 35 after inoculation; tumor volume (mm^3) and body weight (g) were measured twice weekly. No specific physical and behavioral changes were noted in any mice. The average volume of the tumors derived from the M2TRB3 cells was significantly increased by 38% when compared with that of the M2mock tumors at experimental day 35 ($P<0.05$) (Fig. 2B).

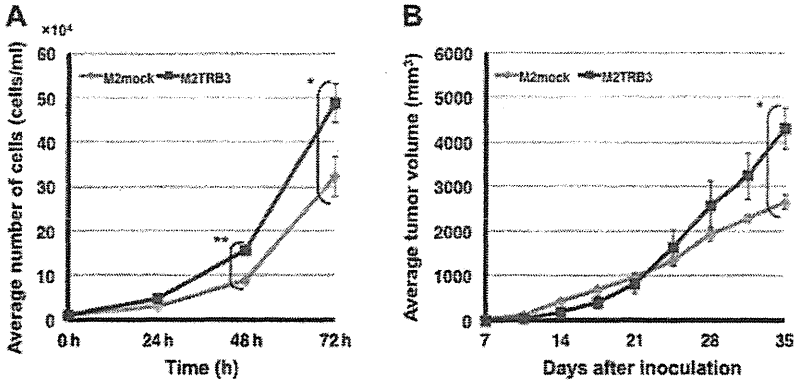

Figure 2. Growth enhancing effects of the TRB3 gene. (A) Growth curve of the cell proliferation assay. Asterisk(s) indicate statistical significance between the two cell lines (*P<0.05, **P<0.01). (B) Volume of the M2TRB3 tumors and M2mock tumors. Asterisk indicates statistical significance in tumor volume between the two tumors (*P<0.05).

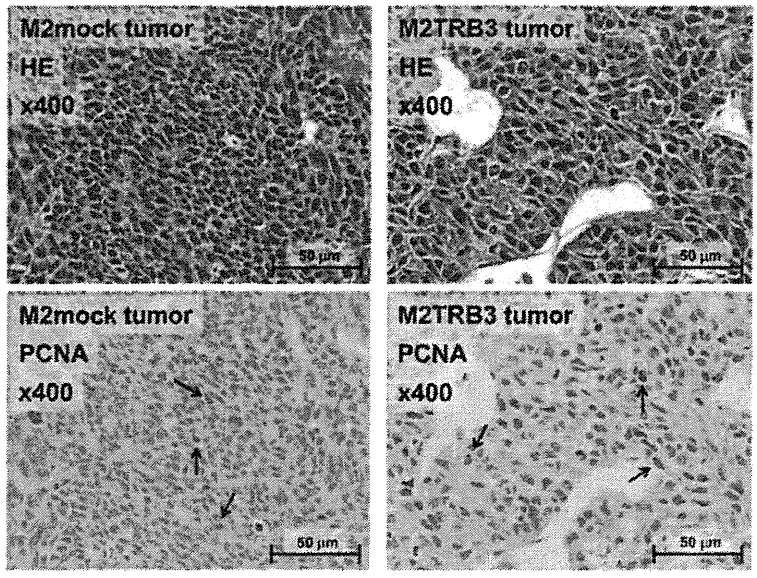

Figure 3. Representative histological features of the M2mock (left rows) and M2TRB3 tumors (right rows). Upper panels were stained with hematoxylin and eosin (HE) and lower panels show immunohistochemical staining of proliferating cell nuclear antigen (PCNA). Approximately 20 and 35% of M2mock and M2TRB3 cells were PCNA-positive (arrows), respectively. Magnification was x400 in all four images.

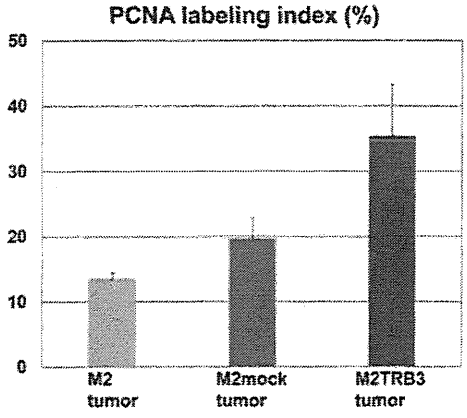

Figure 4. PCNA labeling index in the M2, M2mock and M2TRB tumors. A marked difference was noted between M2mock and M2TRB3 tumors but this difference did not achieve statistical significance.

Gross and histological features and PCNA labeling index of the M2TRB3 tumors. Due to the growth enhancing effects identified above, we aimed to determine whether the TRB3 gene induced morphological changes in tumor tissues. The M2TRB3, M2mock and M2 tumors were excised from the mouse skin, fixed with 10% buffered formalin, and stained with hematoxylin and eosin for histological examination. The tumors were analyzed using a light microscope. M2TRB3 and M2mock tumors presented a pedunculated round shape. Histologically, M2mock tumor cells grew in a solid appearance (Fig. 3, left upper panel). A site of necrosis was present in the central region of the tumor. M2TRB3 tumors were also solid and papillary growth was partially noted (Fig. 3, right upper panel). In the M2TRB3 tumors, the mean diameter of the nucleus (9.4±0.3 μm) was significantly greater than that (7.0±0.2 μm) of the M2mock tumors (P<0.001). The cell proliferation rate was evaluated by measuring the PCNA

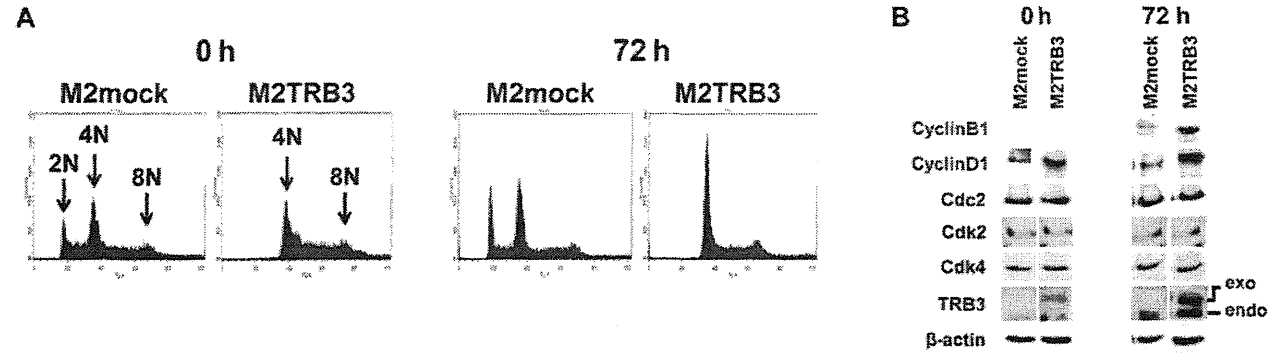

Figure 5. Effects of the TRB3 gene on DNA ploidy and protein expression. (A) Representative results of the flow cytometric analysis. After synchronizing cells in the G0/G1 phase, ploidy status was determined by flow cytometric analysis at 0 (left two panels) and 72 h (right two panels) in the M2mock and M2TRB3 cell lines. Note three peaks (2N, diploid; 4N, tetraploid; 8N, octaploid) in different locations in the DNA histogram. (B) Protein expression status of cell cycle control molecules and TRB3 in M2mock and M2TRB3 cell lines. Cell lysates were extracted at the indicated times (h) of the cell culture and then examined by western blot analysis for the indicated proteins, using the respective antibodies, as described in Materials and methods. β-actin was used as an internal control. Exogenous human TRB3 and endogenous mouse TRB3 are describes as exo and endo, respectively.

Table I. Distribution and rate (%) of ploidy in the M2TRB3 and M2mock cell lines.

		Time (h) after starvation	
Cell line	Ploidy	0 h	72 h
M2mock	2N	12.1±0.3[a]	16.6±0.1[b]
M2TRB3	2N	0.0±0.0	0.0±0.0
M2mock	4N	37.0±0.1	38.5±0.2[b]
M2TRB3	4N	41.6±2.5	57.5±0.5
M2mock	8N	6.0±0.1[a]	3.5±0.0[b]
M2TRB3	8N	25.3±1.8	16.2±0.3

Differences in the percentage of ploidy in M2TRB3 and M2mock cell lines. M2TRB3 vs. M2mock, [a]P<0.01 and [b]P<0.001.

labeling index as described in Materials and methods. The PCNA labeling index of the M2TRB3 tumors was higher than that of the M2 and M2mock tumors but this difference was not statistically significant (Fig. 3 lower panels and Fig. 4).

TRB3 affects the ploidy distribution of mouse mammary tumor cells. Due to the differences in tumor morphology noted in Fig. 3, we examined the effects of the TRB3 gene on DNA ploidy in M2mock and M2TRB3 cells. After synchronizing cells in the G0/G1 phase, we conducted experiments at 0 and 72 h using flow cytometric analysis. Representative DNA histograms of the analysis for these cells are shown in Fig. 5A, and distribution and rate of DNA ploidy are shown in Table I. In M2mock cells, the average percentage of diploid nuclei measured 12-16%. In contrast, no diploid nuclei were observed in M2TRB3 cells (Table I and Fig. 5A, far right panels). M2TRB3 cells showed a significant increase by 19 and 12% in the population of octaploid nuclei at 0 and 72 h, respectively, when compared to M2mock cells (Table I). There was also an increase (4-19%) in the population of tetraploid nuclei in the M2TRB3 cells. These results indicate that TRB3 affects the status of DNA ploidy in mouse mammary tumor cells. M2mock cells exhibited population peaks of aneuploid nuclei (2N, 4N and 8N), indicating that these cells harbor a variable number of chromosomes.

Expression status of TRB3 and cell cycle control molecules in M2TRB3 and M2mock cells. Due to the growth enhancing effects of TRB3 as noted in Fig. 2 and nuclear hyperploidy in M2TRB3 cells, we examined whether these cells affected the levels of expression of TRB3 and cell cycle control molecules. Thus, we measured the protein expression levels of TRB3 and cell cycle control molecules cyclin B1, cyclin D1, Cdc2, Cdk2 and Cdk4. In M2TRB3 cells, both exogenous and endogenous TRB3 were highly expressed at 72 h compared to M2mock cells that only expressed endogenous TRB3 (Fig. 5B, right two columns). In contrast, a weak expression level of endogenous TRB3 was observed at 0 h in the M2mock cells, and marginal expression was noted in both exogenous and endogenous TRB3 at the same time point in these cells. Cyclin B1 and cyclin D1 expression levels in the M2TRB3 cells increased at 72 h of the cell culture, in which tumor cells were out of synchrony, compared to those of the M2mock cells (Fig. 5B). Expression levels of Cdc2, Cdk2, and Cdk4 showed no change between the M2TRB3 and M2mock cells.

Discussion

Several human tumor tissues have recently been shown to highly express TRB3 mRNA (14). It has also been demonstrated by us that TRB3 regulates the stability of Cdc25A, an essential activator of CDKs (10). However, the precise role and functional morphology of TRB3 have not been established yet. Thus, we carried out the present study to provide further evidence concerning cell growth and morphological changes in mouse mammary tumor cells by focusing on the expression levels of TRB3 and cell cycle control molecules, cellular nucleus size, and the status of DNA ploidy. M2TRB3 cells showed a significant numerical increase compared to the control M2mock cells. As a result, the doubling time of the M2TRB3 and M2mock cell lines was approximately 12

and 15 h, respectively (Fig. 2A). A similar condition was also observed in the tumors, clearly indicating that in this context TRB3 had an enhancing property on the growth of mouse mammary tumor cells.

It is well understood that cell volume increases with DNA ploidy, and this correlation has been observed in a wide variety of eukaryotic cells (19). Increased DNA ploidy can exert its effects by increasing nuclear size, chromatin content, and the expression levels of a certain gene (19). We found that in the M2TRB3 tumors the mean diameter of the nucleus measured 9.4±0.3 μm and that of the M2mock tumors was 7.0±0.2 μm. From the flow cytometric analysis we also found a significant increase in the population of M2TRB3 cells bearing tetraploid or octaploid nuclei compared to that of the M2mock cells bearing mostly diploid or tetraploid nuclei (Fig. 5A). These findings are consistent with those reported by Danielsen *et al* (20) who demonstrated that nuclei of 6.0-7.5 μm in diameter are classified as diploid, 7.5-9.0 μm as tetraploid, and 9.5-11.0 μm as octaploid. Collectively, TRB3 may have the ability of polyploidization during development.

Cyclins are the key molecules in cell cycle control due to their specific and periodic expression during cell cycle progression. Cyclin D1 complexes with Cdk4 and Cdk6 and thereby regulates transition from the G1 phase into the S phase by phosphorylation and inactivation of pRB (21-24). Phosphorylation causes release of the transcription factor E2F that promotes mitosis (24,25). Gene amplification and/or protein overexpression of cyclin D1 occurs in a variety of human carcinomas and tumors in animal models (26,27). Unlike cyclin D1, the activity of cyclin B1 is essential for G2/M phase of the cell cycle through a complex with Cdc2 (28). However, little is known about the association between DNA ploidy and cyclin B1/cyclin D1 expression status. We found elevated expression levels of cyclin B1 and cyclin D1 in M2TRB3 cells without significant changes in expression levels of Cdc2, Cdk2 and Cdk4 (Fig. 5B). Furthermore, M2TRB3 cells totally lack diploid nuclei but a population of the M2mock cells consisted mainly of diploid or tetraploid nuclei, suggesting that expression of cyclin B1 and cyclin D1 may positively correlate with the generation of hyperploid nuclei and thereby further promote the chromosomal instability in TRB3-overexpressing cells. Similar results regarding cyclin B1/D1 overexpression and promotion of tetraploidy or aneuploidy (>2N) were previously obtained in human breast carcinoma and mouse myeloid cells (28,29). As we found in the present study, the novel aspect of the TRB3 gene is that this gene induces an increase in cell proliferation and polyploidy leading to enlargement of the nuclear size of the implanted mouse mammary tumor cells. These effects of TRB3 may cause chromosomal instability. The detailed mechanism of this chromosomal instability is not known but may be related to the above-described effects of TRB3 on morphological function. In a recent study, we demonstrated that TRB3 may regulate the activity of anaphase-promoting complex/cyclosome (APC/C^{Cdh1}) that is a major ubiquitin ligase complex regulating the progression of the cell cycle through the ubiquitination and subsequent degradation of cell cycle control molecules including cyclin B1 (30,31). In the present study, we found an elevated expression level of the cyclin B1 protein in M2TRB3 cells that overexpressed the human TRB3 gene. We should emphasize that two cell lines M2TRB3 and M2mock differ in synchrony status that may influence their response to morphological function. This intriguing respect may also reflect the role of cell cycle progression of TRB3. Thus, it is of interest to examine whether the TRB3 gene causes *de novo* morphological changes leading to tumorigenesis in a specific organ site. An additional study using the TRB3 transgenic animal model is currently in progress to answer this question.

Acknowledgements

We thank Dr Hiroyuki Tsuda for the valuable comments and discussions. We also acknowledge the excellent technical assistance of Kenta Moriwaki and Shuhei Ikenaga. This study was supported by a Grant-in-Aid from the Ministry of Education, Culture, Sports, Science, and Technology, and the Ministry of Health, Labour, and Welfare of Japan.

References

1. Grosshans J and Wieschaus E: A genetic link between morphogenesis and cell division during formation of the ventral furrow in *Drosophila*. Cell 101: 523-531, 2000.
2. Mata J, Curado S, Ephrussi A and Rørth P: Tribbles coordinates mitosis and morphogenesis in *Drosophila* by regulating string/CDC25 proteolysis. Cell 101: 511-522, 2000.
3. Seher TC and Leptin M: Tribbles, a cell-cycle brake that coordinates proliferation and morphogenesis during *Drosophila* gastrulation. Curr Biol 10: 623-629, 2000.
4. Bowers AJ, Scully S and Boylan JF: SKIP3, a novel *Drosophila* tribbles ortholog, is overexpressed in human tumors and is regulated by hypoxia. Oncogene 22: 2823-2835, 2003.
5. Bezy O, Vernochet C, Gesta S, Farmer SR and Kahn CR: TRB3 blocks adipocyte differentiation through the inhibition of C/EBPβ transcriptional activity. Mol Cell Biol 27: 6818-6831, 2007.
6. Chan MC, Nguyen PH, Davis BN, Ohoka N, Hayashi H, Du K, Lagna G and Hata A: A novel regulatory mechanism of the bone morphogenetic protein (BMP) signaling pathway involving the carboxyl-terminal tail domain of BMP type II receptor. Mol Cell Biol 27: 5776-5789, 2007.
7. Du K, Herzig S, Kulkarni RN and Montminy M: TRB3: a tribbles homolog that inhibits Akt/PKB activation by insulin in liver. Science 300: 1574-1577, 2003.
8. Qi L, Heredia JE, Altarejos JY, Screaton R, Goebel N, Niessen S, Macleod IX, Liew CW, Kulkarni RN, Bain J, Newgard C, Nelson M, Evans RM, Yates J and Montminy M: TRB3 links the E3 ubiquitin ligase COP1 to lipid metabolism. Science 312: 1763-1766, 2006.
9. Tang M, Zhong M, Shang Y, Lin H, Deng J, Jiang H, Lu H, Zhang Y and Zhang W: Differential regulation of collagen types I and III expression in cardiac fibroblasts by AGEs through TRB3/MAPK signaling pathway. Cell Mol Life Sci 65: 2924-2932, 2008.
10. Ohoka N, Yoshii S, Hattori T, Onozaki K and Hayashi H: TRB3, a novel ER stress-inducible gene, is induced via ATF4-CHOP pathway and is involved in cell death. EMBO J 24: 1243-1255, 2005.
11. Sakai S, Ohoka N, Onozaki K, Kitagawa M, Nakanishi M and Hayashi H: Dual mode of regulation of cell division cycle 25 A protein by TRB3. Biol Pharm Bull 33: 1112-1116, 2010.
12. Jin G, Yamazaki Y, Takuwa M, Takahara T, Kaneko K, Kuwata T, Miyata S and Nakamura T: Trib1 and Evi1 cooperate with Hoxa and Meis1 in myeloid leukemogenesis. Blood 109: 3998-4005, 2007.
13. Keeshan K, He Y, Wouters BJ, Shestova O, Xu L, Sai H, Rodriguez CG, Maillard I, Tobias JW, Valk P, Carroll M, Aster JC, Delwel R and Pear WS: Tribbles homolog 2 inactivates C/EBPα and causes acute myelogenous leukemia. Cancer Cell 10: 401-411, 2006.
14. Xu J, Lv S, Qin Y, Shu F, Xu Y, Chen J, Xu BE, Sun X and Wu J: TRB3 interacts with CtIP and is overexpressed in certain cancers. Biochim Biophys Acta 1770: 273-278, 2007.

15. Suzui M, Sunagawa N, Chiba I, Moriwaki H and Yoshimi N: Acyclic retinoid, a novel synthetic retinoid, induces growth inhibition, apoptosis, and changes in mRNA expression of cell cycle- and differentiation-related molecules in human colon carcinoma cells. Int J Oncol 28: 1193-1199, 2006.
16. Suzui M, Inamine M, Kaneshiro T, Morioka T, Yoshimi N, Suzuki R, Kohno H and Tanaka T: Indole-3-carbinol inhibits the growth of human colon carcinoma cells but enhances the tumor multiplicity and volume of azoxymethane-induced rat colon carcinogenesis. Int J Oncol 27: 1391-1399, 2005.
17. Suzui M, Masuda M, Lim JT, Albanese C, Pestell RG and Weinstein IB: Growth inhibition of human hepatoma cells by acyclic retinoid is associated with induction of p21(CIP1) and inhibition of expression of cyclin D1. Cancer Res 62: 3997-4006, 2002.
18. Futakuchi M, Nannuru KC, Varney ML, Sadanandam A, Nakao K, Asai K, Shirai T, Sato SY and Singh RK: Transforming growth factor-beta signaling at the tumor-bone interface promotes mammary tumor growth and osteoclast activation. Cancer Sci 100: 71-81, 2009.
19. Jorgensen P and Tyers M: How cells coordinate growth and division. Curr Biol 14: 1014-1027, 2004.
20. Danielsen H, Lindmo T and Reith A: A method for determining ploidy distributions in liver tissue by stereological analysis of nuclear size calibrated by flow cytometric DNA analysis. Cytometry 7: 475-480, 1986.
21. Hunter T and Pines J: Cyclins and cancer. II: cyclin D and CDK inhibitors come of age. Cell 79: 573-582, 1994.
22. Weinberg RA: The retinoblastoma protein and cell cycle control. Cell 81: 323-330, 1995.
23. Chellappan SP, Hiebert S, Mudryj M, Horowitz JM and Nevins JR: The E2F transcription factor is a cellular target for the RB protein. Cell 65: 1053-1061, 1991.
24. Wilson CS, Butch AW, Lai R, Medeiros LJ, Sawyer JR, Barlogie B, McCourty A, Kelly K and Brynes RK: Cyclin D1 and E2F-1 immunoreactivity in bone marrow biopsy specimens of multiple myeloma: relationship to proliferative activity, cytogenetic abnormalities and DNA ploidy. Br J Haematol 112: 776-782, 2001
25. Johnson DG, Schwarz JK, Cress WD and Nevins JR: Expression of transcription factor E2F1 induces quiescent cells to enter S phase. Nature 365: 349-352, 1993.
26. Staibano S, Lo Muzio L, Pannone G, Mezza E, Argenziano G, Vetrani A, Lucariello A, Franco R, Errico ME and De Rosa G: DNA ploidy and cyclin D1 expression in basal cell carcinoma of the head and neck. Am J Clin Pathol 115: 805-813, 2001.
27. Bartkova J, Lukas J, Strauss M and Bartek J: Cyclin D1 oncoprotein aberrantly accumulates in malignancies of diverse histogenesis. Oncogene 10: 775-778, 1995.
28. Collecchi P, Santoni T, Gnesi E, Giuseppe Naccarato A, Passoni A, Rocchetta M, Danesi R and Bevilacqua G: Cyclins of phases G1, S and G2/M are overexpressed in aneuploid mammary carcinomas. Cytometry 42: 254-260, 2000.
29. Yin XY, Grove L, Datta NS, Katula K, Long MW and Prochownik EV: Inverse regulation of cyclin B1 by c-Myc and p53 and induction of tetraploidy by cyclin B1 overexpression. Cancer Res 61: 6487-6493, 2001.
30. Ohoka N, Sakai S, Onozaki K, Nakanishi M and Hayashi H: Anaphase-promoting complex/cyclosome-cdh1 mediates the ubiquitination and degradation of TRB3. Biochem Biophys Res Commun 392: 289-294, 2010.
31. Lukas C, Sørensen CS, Kramer E, Santoni-Rugiu E, Lindeneg C, Peters JM, Bartek J and Lukas J: Accumulation of cyclin B1 requires E2F and cyclin-A-dependent rearrangement of the anaphase-promoting complex. Nature 401: 815-818, 1999.

Carcinogenesis Advance Access published March 11, 2013

Carcinogenesis vol.00 no.00 p.1 of 9, 2013
doi:10.1093/carcin/bgt053
Advance Access publication February 7, 2013

Metabolomic and transcriptomic profiling of human K-*ras* oncogene transgenic rats with pancreatic ductal adenocarcinomas

Setsuko Yabushita[1,*], Katsumi Fukamachi[2], Hajime Tanaka[3], Takako Fukuda[1], Kayo Sumida[1], Yoshihito Deguchi[1], Kazuki Mikata[1], Kazuhiko Nishioka[1], Satoshi Kawamura[1], Satoshi Uwagawa[1], Masumi Suzui[2], David B.Alexander[2,4] and Hiroyuki Tsuda[4]

[1]Environmental Health Science Laboratory, Sumitomo Chemical Co., Osaka 554-8558, Japan, [2]Department of Molecular Toxicology, Nagoya City University Graduate School of Medical Sciences, Nagoya 467-8601, Japan, [3]Department of Gastroenterology and Metabolism, Nagoya City University Graduate School of Medical Sciences, Nagoya 467-8601, Japan and [4]Nanotoxicology Project, Nagoya City University, Nagoya 467-8603, Japan

*To whom correspondence should be addressed. Tel: +81-66466-5306; Fax: +81-66466-5319;
Email: yabushitas@sc.sumitomo-chem.co.jp

Pancreatic ductal adenocarcinoma (PDAC) is one of the most debilitating malignancies in humans, and one of the reasons for this is the inability to diagnose this disease early in its development. To search for biomarkers that can be used for early diagnosis of PDAC, we established a rat model of human PDAC in which expression of a human K-*rasG12V* oncogene and induction of PDAC are regulated by the *Cre/lox* system. In the present study, transgenic rats bearing PDAC and control transgenic rats with normal pancreatic tissues were used for metabolomic analysis of serum and pancreatic tissue by non-targeted and targeted gas chromatography–mass spectrometry and transcriptomic analysis of pancreatic tissue by microarray. Comparison of the metabolic profiles of the serum and pancreatic tissue of PDAC-bearing and control rats identified palmitoleic acid as a metabolite, which was significantly decreased in the serum of PDAC-bearing animals. Transcriptomic analysis indicated that several transcripts involved in anaerobic glycolysis and nucleotide degradation were increased and transcripts involved in the trichloroacetic acid cycle were decreased. Other transcripts that were changed in PDAC-bearing rats were adenosine triphosphate citrate lyase (decreased: fatty acid biosynthesis), fatty acid synthase (increased: fatty acid biosynthesis) and arachidonate 5-lipoxygenase activating protein (increased: arachidonic acid metabolism). Overall, our results suggest that the decreased serum levels of palmitoleic acid in rats with PDAC was likely due to its decrease in pancreatic tissue and that palmitoleic acid should be investigated in human samples to assess its diagnostic significance as a serum biomarker for human PDAC.

Introduction

Pancreatic cancer is diagnosed in ~1 person per 10 000 annually in the USA and is the fifth leading cause of cancer mortality. Most patients die within 1 year of diagnosis, and the 5 year survival rate, less than 5%, is dismal (1). Pancreatic ductal adenocarcinomas (PDACs) are diagnosed in ≥95% of the patients with pancreatic cancer. The most widely used marker for pancreatic cancer, CA19-9, lacks specificity and sensitivity: it is elevated in cases of benign cholangitis and pancreatitis and also in other types of cancer, and it is not elevated during the early stages of PDAC, when the lesion is potentially curable (2–4). Thus, there are presently no reliable biomarkers for the early detection of pancreatic cancer. Consequently, there is an urgent need for specific and sensitive biomarkers of pancreatic cancer.

Previously, we established transgenic rats in which expression of the human H-*ras*^{G12V} or K-*ras*^{G12V} oncogene is regulated by the *Cre/lox* system (5). Targeted activation of H-*ras*^{G12V} or K-*ras*^{G12V} is accomplished by injection of a *Cre*-carrying adenovirus into the pancreatic ducts through the common bile duct. Several weeks after injection, proliferative lesions in pancreatic duct epithelium, intercalated ducts and centroacinar cells, but not acinar cells, become widespread. The histopathological appearance of these adenocarcinomas closely resembles that described for typical pancreatic tumors in man. Thus, transgenic rats with induced PDACs in pancreatic tissues are an appropriate model for human PDAC. In this study, K-*ras*^{G12V} transgenic rats (K-*ras*^{G12V} Tg rats) were used because K-*ras* mutations are commonly observed in human PDAC.

Serum/plasma biomarkers are ideal in that the collection of samples is relatively non-invasive, and samples can be obtained repeatedly to monitor disease progression. Molecular profiling approaches such as transcriptomics, proteomics and metabolomics to monitor pathological processes of disease have received a great deal of attention. Metabolomic analysis refers to the comprehensive study of the many metabolites present in biological samples (6,7). The analytical techniques typically applied are nuclear magnetic resonance (8) and mass spectrometry (9), with the latter being coupled to chromatographic separation techniques such as gas chromatography or liquid chromatography. Metabolomics is a powerful method for screening biomarkers, interpreting biological pathways and understanding functions of complex biological systems (10). Recently, a urinary biomarker of prostate cancer aggressiveness was found using metabolomic profiling (11).

In the present study, we characterized the metabolite profiles of both serum and pancreatic tissue samples from control and PDAC-bearing K-*ras*^{G12V} Tg rats by non-targeted and targeted gas chromatography–mass spectrometry (GC-MS) analysis to identify potential serum biomarkers for the clinical diagnosis of PDAC. In addition, the metabolomic analysis was integrated with a transcriptomic analysis of pancreatic tissues to obtain a better understanding of the behavior of metabolites in PDAC. We identified palmitoleic acid as a metabolite that was significantly decreased in the serum of rats with PDAC, and integrated metabolomic and transcriptomic analyses suggest fluctuations in several metabolomic pathways in PDAC lesions.

Abbreviations: Acly, adenosine triphosphate citrate lyase; Alox5ap, arachidonate 5-lipoxygenase activating protein; Fasn, fatty acid synthase; GC-MS, gas chromatography–mass spectrometry, PCA, principal component analysis; PDAC, pancreatic ductal adenocarcinoma; TCA, trichloroacetic acid; TIC, total ion current.

Materials and methods

Ethics statement

All experiments were conducted in accordance with the 'Guidelines for Animal Experiments of Nagoya City University Graduate School of Medical Sciences', and the experimental protocol was approved by the Nagoya City University Medical School Institutional Animal Care and Use Committee.

Induction of pancreatic ductal adenocarcinoma

Kras301 rats conditionally expressing human K-*ras*^{G12V} were generated as described previously (12). An adenovirus vector carrying the *Cre* gene (AxCANCre) and an empty adenovirus vector (AxCAwt) were injected into the pancreatic ducts of 10–11-week-old adult homozygous male Kras301 rats through the common duct as described previously (5,12). Six rats were treated with AxCANCre (PDAC rats) and four with AxCAwt (as controls). All rats were maintained in plastic cages in an air-conditioned room with a 12 h light/12 h dark cycle and euthanized by blood withdrawal from the abdominal aorta under anesthesia 16–17 days after the injection of adenovirus vector.

Collection of pancreatic tissue and serum

Rats were killed by exsanguination under ether anesthesia. Immediately after exsanguination, pancreatic tissues were excised from euthanized rats, cut into portions and the portions either frozen in liquid nitrogen or processed for

pathological examination (see below). Collected blood samples were allowed to clot at room temperature and then centrifuged at 3000 r.p.m. for 10 min at 4°C to obtain serum. The frozen pancreatic tissues and the serum were stored in liquid nitrogen and at −80°C, respectively, until metabolomic analysis.

Pathological examination

The remaining pancreatic tissues from PDAC and control rats were fixed in 4% paraformaldehyde, processed for embedding in paraffin, cut into 3 μm sections and stained with hematoxylin and eosin for microscopic examination.

RNA extraction from pancreatic tissues

Extraction of total RNA was performed using an RNeasy Mini Kit (Qiagen, Hilden, Germany). Quantification was performed with an Amersham Pharmacia spectrophotometer, model Ultraspec 3100pro (Amersham Pharmacia Biotech, Uppsala, Sweden), and assessment of ribosomal RNA integrity was performed using a 2100 Bioanalyzer (Agilent Technologies, Palo Alto, CA). Total RNA samples were stored at −80°C immediately after extraction.

Gene expression analysis

Gene expression levels were measured using a GeneChip System (Affymetrix, Santa Clara, CA). Reverse transcription of the extracted total RNA, second-strand synthesis and probe generation were all accomplished with One-Cycle Target Labeling and Control Reagents (Affymetrix) following the manufacturer's protocol. Briefly, from 5 μg of total RNA, first-strand cDNA was synthesized with SuperScript II reverse transcriptase and a T7-oligo (dT) primer, and double-strand cDNA was synthesized with *Escherichia coli* RNase H, *E.coli* DNA polymerase I and *E.coli* DNA ligase. Biotin-labeled cRNA was prepared from the double-strand cDNA, and 15 μg of labeled cRNA was fragmented. Rat Genome 230 2.0 arrays were hybridized as described in the Gene Chip Expression Analysis Technical Manual (Affymetrix). The arrays were stained and washed with R-Phycoerythrin Streptavidin (Molecular Probes, Eugene, OR) and with the GeneChip Hybridization, Wash, and Stain Kit (Affymetrix). Fluorescence was intensified by the antibody-amplification method. The arrays were scanned with a GeneChip Scanner 3000 (Affymetrix) with Affymetrix Genechip Command Console (AGCC) and the image files were analyzed with an Affymetrix data suite system, Expression Console (EC) version 1.1; the tab-delimited files obtained contained data regarding the relative levels of expression of transcripts (signal) and the reliability of detection (Detection Call). The derived signal values were globally normalized to 100.

Sample preparation for GC-MS analysis

Pancreatic tissue and serum were subjected to two derivatization steps for GC-MS analysis. Pancreatic tissue samples (45–84 mg) were weighed and homogenized in a 12-fold volume solution of methanol/water/10 mM 2-hydroxyundecanoic acid (800:100:1, v/v/v; 10 mM 2-hydroxyundecanoic acid was used as an internal standard) using a potter homogenizer on ice, followed by centrifugation at 15 000 r.p.m. for 10 min at 4°C. Serum samples (50 μl) were deproteinized by addition of an 8-fold volume solution of methanol/water/10 mM 2-hydroxyundecanoic acid (800:100:1, v/v/v; 10 mM 2-hydroxyundecanoic acid was used as an internal standard), followed by centrifugation at 15 000 r.p.m. for 5 min at 4°C. The supernatant (200 μl) was dried in a vacuum freeze dryer, 30 μl of methoxylamine hydrochloride (Sigma–Aldrich) in pyridine (10 mg/ml) was added as a derivatizing agent and the mixture was incubated at 30°C for 90 min. Thereafter, 30 μl of *N*-methyl-*N*-(trimethylsilyl)trifluoroacetamide (GL Science, Tokyo, Japan) was added for derivatization, and the mixture was incubated at 40°C for 30 min.

GC-MS analysis

All analyses were carried out with a Bruker Daltonics1200 GC/MS/MS system (Bruker Daltonics K.K., Japan) using an Agilent Technologies VF5-ms capillary column (length, 30 m; internal diameter, 0.25 mm; film thickness, 0.25 μm). The injection temperature was 230°C. The helium gas flow rate through the column was 1 ml/min. The column oven temperature was 60°C for 2 min and rose at 10°C/min to 300°C and then remained at 300°C for 5 min. Ions were generated at an electron impact energy of 70 kV and were recorded over the mass range from *m/z* 70 to 800.

Analysis of GC-MS data

GC-MS data were imported into LineUp (Infometrix, Bothell, WA) and PiroTrans (GL Science) in order to align the chromatogram on the basis of peak intensity and the retention time of the internal standard, 2-hydroxyundecanoic acid. The generated peak lists were imported into Pirouette software (Infometrix, Woodinville, WA) for multivariate statistical analysis. Principal component analysis (PCA) was conducted to find discriminatory metabolites in serum and pancreatic tissues of PDAC rats. Identification of discriminatory metabolites detected by PCA analysis was performed using the NIST 05 Mass Spectral Library (NIST) containing >200 000 electron impact spectra. In addition to the automatic library search assessment on the basis of similarity score (>65), the similarity of spectra was manually confirmed.

Identification and quantification of palmitoleic acid in pancreatic tissues

To authenticate the identity of the metabolite putatively identified as palmitelaidic acid, pancreatic tissues were analyzed by cochromatography with palmitelaidic acid and palmitoleic acid standards (MP Biomedicals, CA). The identity of the metabolite was determined based on comparison of the retention time and fragment pattern of the metabolite and those of the two standards.

For concentration measurements, palmitoleic acid was diluted in pyridine and six standards of various mixtures of compounds of known concentration between 0.05 and 100 p.p.m. were prepared. The concentration of palmitoleic acid in the samples was quantified by a standard curve of total ion current (TIC) chromatograms or *m/z* 311 mass chromatograms.

Statistics

The peak intensities of metabolites and the signal values of gene expression were statistically analyzed by the Student's *t*-test between PDAC and control rats, with a level of probability of 0.05 used as the criterion for significance.

Results

Gross and histological observation

Kras301 rats, 13–14 weeks of age, were killed 16–17 days after injection of adenovirus vector into the pancreatic duct via the common bile duct. Gross and histological findings were the same as reported previously (5,12,13). PDAC was well developed with grossly visible whitish lesions in all six rats treated with AxCANCre. Histopathological examination showed that the tumors were adenocarcinomas with a variable amount of fibrotic tissue, some showing desmoplastic morphology and infiltration of inflammatory cells. Invasion of the surrounding normal pancreatic tissue by the PDAC that developed in Kras301 rats was a common feature of these lesions. Figure 1 shows typical lesions that developed in the Kras301 rats.

PDAC that develop in Kras301 rats are not metastatic, and neoplastic lesions were not found in any other organs. No abnormalities were observed in pancreatic tissues of the four rats injected with AxCAwt.

GC-MS chromatograms of serum and pancreatic tissues

Typical GC-MS TIC chromatograms of serum and pancreatic tissue extracts are shown in Supplementary Figure 1, available at *Carcinogenesis* Online. The retention time of the internal standard was consistent for each run. The data showed marked differences in the chromatogram patterns between the serum and pancreatic tissue.

Clustering of control and PDAC samples

Score plots produced by PCA of the serum pancreatic tissue are shown in Figure 2. The PCA algorithm generates a single point that represents the metabolites in a sample and their concentrations (each dot in the score plots shown in Figure 2 represents a single rat); close clustering of dots indicates that the samples have similar compositions. The control and PDAC samples clustered into two distinct groups in both the serum (Figure 2A) and pancreatic tissue (Figure 2B) score plots, indicating that the profiles of the metabolites in the serum and pancreatic tissue samples derived from the control rats differed from those derived from the rats with PDAC.

Metabolite differences between control and PDAC samples screened by PCA

In addition to the score plot, which is based on the composition of the samples, the PCA algorithm also creates a loading plot, which is based on metabolite values. Loading plots identify metabolites that contribute to the differential clustering of PDAC and control samples in the score plots. The electron impact spectra of these discriminatory metabolites were then compared with the NIST 05 Mass Spectral Library (NIST). Putatively identified discriminatory metabolites with matching NIST spectra are shown in Table I. Fold changes and *P*-values of these metabolites in the serum and pancreatic tissues were calculated by the TICs of GC-MS chromatograms.

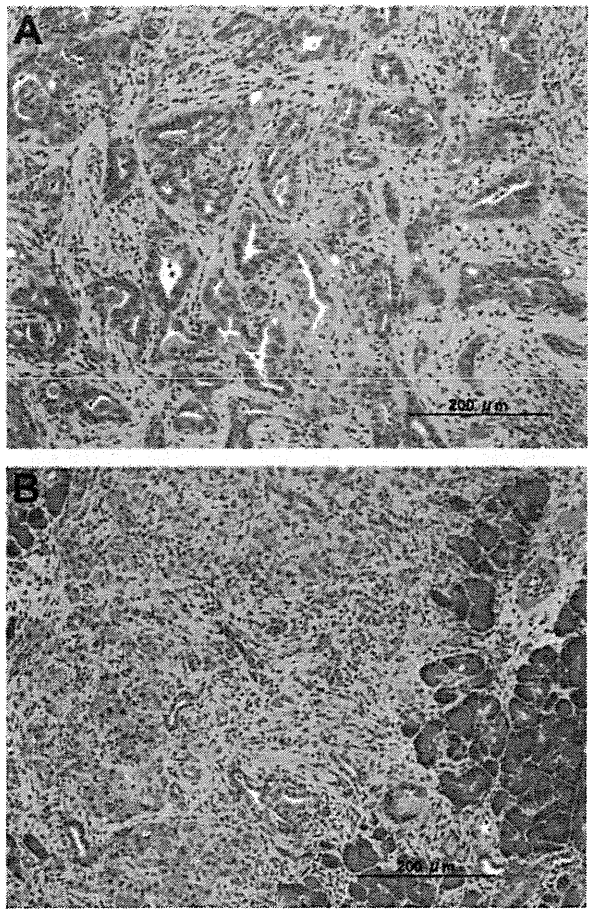

Fig. 1. Typical lesions that developed in the Kras301 rats are shown. (**A**) An adenocarcinoma with desmoplastic appearance. (**B**) An adenocarcinoma invading the surrounding pancreas tissue.

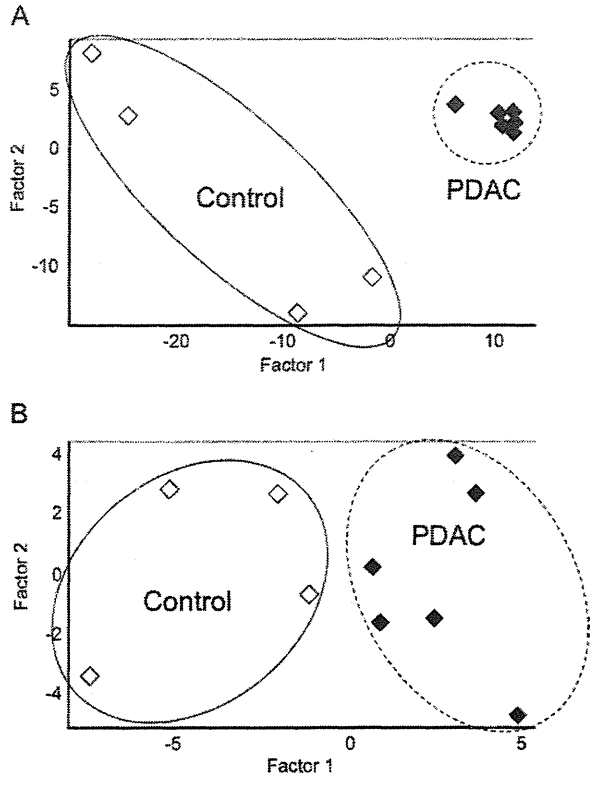

Fig. 2. Score plots of PCA based on the metabolite profile data of PDAC rats and control rats. The rhombus plots (filled and open) indicate the results for PDAC rats ($n = 6$) and control rats ($n = 4$), respectively. (**A**) Score plots of PCA based on the metabolite profile data for pancreatic tissues discriminating between PDAC and control rats. The principal components PC1 ($t[1]$) and PC2 ($t[2]$) described 59.6 and 14.9% of the variation. (**B**) Score plots of PCA based on the metabolite profile data of serum discriminating between PDAC and control rats. The principal components PC1 ($t[1]$) and PC2 ($t[2]$) described 32.8 and 18.0% of the variation.

In the serum, aminomalonic acid, 2-aminoethyl dihydrogen phosphate, citrate and lanthionine were significantly increased and chenodeoxycholic acid was non-significantly increased (1.9-fold). In pancreatic tissues, however, none of these metabolites was significantly increased and aminomalonic acid was significantly decreased.

A number of fatty acids were decreased in pancreatic tissues: palmitelaidic acid, linoleic acid, octadecanoic acid, myristic acid, arachidonic acid and hexadecanoic acid were significantly decreased and tridecanoic acid, 12-methyl-, methyl ester and heptadecanoic acid were non-significantly decreased. Of these fatty acids, only palmitelaidic acid (significantly decreased) and arachidonic acid (non-significantly decreased) were also decreased in the serum.

A third metabolite that had corresponding fluctuations in both the serum and pancreatic tissue was 2(1*H*)-pyrimidinone. This metabolite was significantly decreased in pancreatic tissues and non-significantly in the serum.

None of the other discriminatory metabolites had corresponding fluctuations in both the serum and pancreatic tissue. Beta-alanine, xanthine and uridine were increased in pancreatic tissue but not in the serum, and aspartic acid, alpha-glycerophosphoric acid, tyrosine, 2-monopalmitin, adenosine monophosphate and purine were decreased in pancreatic tissue but not in the serum.

Overall, the metabolic profiles in the pancreatic tissue and the serum of control and PDAC-bearing rats were different, with several discriminatory metabolites contributing to this difference. The array of changes in the individual discriminatory metabolites in the serum and pancreatic tissue, however, were distinct.

Identification and quantification of palmitoleic acid in pancreatic tissue and serum using standard chemicals

Once a metabolite that was significantly decreased in both pancreatic tissues and serum was detected and putatively identified as palmitelaidic acid, the identification of the metabolite was authenticated by cochromatography with palmitelaidic acid and palmitoleic acid. The retention time and fragment pattern of the standards identified the putatively annotated palmitelaidic acid as 'palmitoleic acid'.

A standard curve was then used for concentration measurement in samples: the linear region of quantitation was between 0.1 and 100 p.p.m. ($R^2 = 0.9857$). The concentrations of palmitoleic acid in pancreatic tissues and serum of the individual control and PDAC-bearing rats are shown in Table II. The palmitoleic acid concentration in the pancreatic tissues of control and PDAC rats was 266.5 186.2 and 7.5 4.6 p.p.m., respectively, and the concentration of palmitoleic acid in the serum samples of control and PDAC-bearing rats was 2.6 0.8 and 1.2 0.1 p.p.m., respectively (P-value: 0.031).

Alternations in the levels of metabolites involved in glycolysis and the trichloroacetic acid cycle

The 'Warburg effect' in which tumor cells rapidly use glucose and convert the majority of it to lactate is known as a typical signature of cancer (14,15). Since we observed decreases for a number of fatty acids, which are functionally related to the glycolytic pathway, in the pancreatic tissue of PDAC-bearing rats, we searched for peaks

Table I. Fold changes of the discriminatory metabolites characterizing PDAC tissues and serum

Metabolites	Retention time (min)	Serum		Pancreatic tissues	
		PDAC/control		PDAC/control	
		Fold changes	*P*-values	Fold changes	*P*-values
Threonine	10.37	1.2[a]	0.373	1.3	0.330
Beta-alanine	10.94	ND		1.7[a]	0.072
Aminomalonic acid	11.46	1.3	0.011*	0.8[a]	0.019*
Aspartic acid	12.07	1.3	0.106	0.7[a]	0.005*
Tridecanoic acid, 12-methyl-, methyl ester	14.53	ND		0.1[a]	0.051
Alpha-glycerophosphoric acid	14.79	1.4	0.060	0.8[a]	0.000*
2-Aminoethyl dihydrogen phosphate	15.04	1.2[a]	0.035*	1.0	0.257
Citrate	15.40	1.3[a]	0.017*	1.2	0.522
Tyrosine	16.67	1.2	0.086	0.3[a]	0.024*
Xanthine	17.45	1.1	0.405	1.7[a]	0.016*
Palmitelaidic acid	17.54	0.6[a]	0.002*	0.1[a]	0.001
Heptadecanoic acid	18.62	0.9	0.277	0.3[a]	0.062
Linoleic acid	19.24	0.9	0.683	0.2[a]	0.000*
Octadecanoic acid	19.57	ND		0.7[a]	0.001*
Lanthionine	19.87	1.4[a]	0.027*	1.0	0.949
Myristic acid	20.46	0.9	0.138	0.1[a]	0.020*
Arachidonic acid	20.56	0.4[a]	0.098	0.6[a]	0.021*
Uridine	21.22	ND		3.2[a]	0.001*
2-Monopalmitin	21.97	1.0	0.205	0.05[a]	0.001*
Hexadecanoic acid	22.22	0.9	0.203	0.1[a]	0.038*
2(1*H*)-Pyrimidinone	23.96	0.5	0.316	0.5[a]	0.000*
Adenosine monophosphate	25.55	0.9	0.304	0.5[a]	0.000*
Purine	25.85	ND		0.4[a]	0.000*
Chenodeoxycholic acid	27.14	1.9[a]	0.148	1.1	0.643

Sera and pancreatic tissues from PDAC rats ($n = 6$) and controls ($n = 4$) were analyzed. ND, peaks were not detected.
[a]Metabolites that contributed to the differentiation of PDAC and control samples in the PCA analysis.
*$P < 0.05$.

Table II. Concentration of palmitoleic acid in the tissue and serum of control and PDAC rats

Rat no.	Concentration in tissue or serum (p.p.m.[a])		*t*-Test
Pancreas control			
30	347.72	266.5±186.2	
38	490.90		
50	127.08		
83	100.33		
Pancreas PDAC			
42	10.58	7.5±4.6	0.069
47	2.01		
84	3.78		
86	13.77		
87	4.97		
88	10.18		
Serum control			
30	2.77	2.6±0.8	
38	3.65		
50	1.97		
83	2.10		
Serum PDAC			
42	1.15	1.2±0.1	0.031
47	0.96		
84	1.34		
86	1.28		
87	1.09		
88	1.20		

[a]p.p.m. in tissue is microgram palmitoleic acid per gram tissue and p.p.m. in serum is microgram palmitoleic acid per milliliter serum.

of metabolites involved in glycolysis and the trichloroacetic acid (TCA) cycle. Glucose, pyruvate, lactate, succinate, fumarate, malate and alph-keto-glutarate were identified. The changes in the levels of these metabolites in the serum and pancreatic tissues were calculated by the TICs of GC-MS chromatograms (Table III). No significant differences between PDAC-bearing rats and control rats were found.

Transcriptional changes related to glycolysis, TCA cycle, fatty acid biosynthesis, arachidonic acid metabolism and nucleotide degradation

Transcriptional data for ~31 000 genes in PDAC and control pancreatic tissue were analyzed by microarray; the genes for which significant changes ($P \leq 0.05$) occurred are shown in Supplementary Table 1, available at *Carcinogenesis* Online. Values for enzymes involved in glycolysis, the TCA cycle, fatty acid biosynthesis, arachidonic acid metabolism and nucleotide degradation are shown in Table IV. Changes in Abat, Alox5, Dpyd, Dpys, Nt5, Uox and Upb transcription were evaluated as unclear as their expression levels were too low to be analyzed accurately by microarray analysis.

Pathways generated by integrating the results we obtained from our metabolic and transcriptional analyses are shown in Figure 3. In PDAC lesions, numerous transcripts involved in anaerobic glycolysis were upregulated and most of those involved in the TCA cycle were downregulated (Figure 3A). Transcription of two lipogenic enzymes was also changed in PDAC lesions: adenosine triphosphate citrate lyase (Acly) was decreased and fatty acid synthase (Fasn) was increased (Figure 3A).

Transcripts of arachidonate 5-lipoxygenase activating protein (Alox5ap), which is necessary for activation of Alox5, were increased (Figure 3B). This increase may be associated with the decrease of linoleic acid and arachidonic acid found in the pancreatic tissue of PDAC-bearing rats (Table I).

A number of transcripts involved in purine and pyrimidine nucleotide degradation were increased; however, transcripts involved in pyrimidine nucleotide degradation downstream of beta-alanine degradation were decreased (Figure 3C). Taken together, these changes may be associated with the changes of adenosine monophosphate, xanthine, uridine and beta-alanine found in pancreatic tissue of PDAC-bearing rats.

Table III. Fold changes of the putatively identified metabolites related to glycolysis and the TCA cycle

Metabolites	Retention time (min)	Serum		Pancreatic tissues	
		PDAC/control		PDAC/control	
		Fold changes	*P*-values	Fold changes	*P*-values
Glucose	16.17	1.0	0.510	1.0	0.940
Pyruvate	5.87	1.1	0.177	1.0	0.198
Lactate	5.95	1.0	0.456	1.0	0.373
Succinate	9.46	0.6	0.065	1.1	0.693
Fumarate	9.62	1.1	0.144	ND	
Malate	11.67	0.9	0.803	0.7	0.054
Alpha-ketoglutarate	12.75	1.0	0.832	0.8	0.631

Sera and pancreatic tissues from PDAC rats ($n = 6$) and controls ($n = 4$) were analyzed. ND, not detected.

Table IV. Microarray analysis of mRNA from pancreatic tissues from control and PDAC rats

Gene symbol	Representative public ID	Gene title	Fold	*P*-value
Abat	U29701	4-Aminobutyrate aminotransferase	0.0	0.077[a]
Acly	NM_016987	Adenosine triphosphate citrate lyase	0.6	0.000*
Aco2	NM_024398	Aconitase 2, mitochondrial	0.6	0.000*
Ada	NM_130399	Adenosine deaminase	3.9	0.000*
Adar	NM_031006	Adenosine deaminase, RNA-specific	0.4	0.018*
Adar	BI292196	Adenosine deaminase, RNA-specific	0.8	0.408
Adarb1	NM_012894	Adenosine deaminase, RNA-specific, B1	0.6	0.294
Adarb1	AW253867	Adenosine deaminase, RNA-specific, B1	0.1	0.066
Adarb1	AW522471	Adenosine deaminase, RNA-specific, B1	3.4	0.000*
Adarb2	NM_133302	Adenosine deaminase, RNA-specific, B2	3.3	0.012*
Adat3	AI029510	Adenosine deaminase, tRNA-specific 3, TAD3 homolog (*S. cerevisiae*)	0.4	0.139
Aldh6a1	NM_031057	Aldehyde dehydrogenase 6 family, member A1	0.2	0.001*
Aldoa	NM_012495	Aldolase A, fructose bisphosphate	4.0	0.001*
Aldob	M10149	Aldolase B, fructose bisphosphate	0.0	0.146
Aldoc	NM_012497	Aldolase C, fructose bisphosphate	0.6	0.100
Alox5	NM_012822	Arachidonate 5-lipoxygenase	2.1	0.081[a]
Alox5ap	NM_017260	Arachidonate 5-lipoxygenase activating protein	3.0	0.000*
Ampd1	J02811	Adenosine monophosphate deaminase 1 (isoform M)	0.8	0.707
Ampd2	BE111787	Adenosine monophosphate deaminase 2 (isoform L)	0.7	0.029*
Ampd2	BE100752	Adenosine monophosphate deaminase 2 (isoform L)	1.5	0.068
Ampd3	NM_031544	Adenosine monophosphate deaminase 3	2.6	0.006*
Cda	AA859352	Cytidine deaminase	2.7	0.031*
Cs	NM_130755	Citrate synthase	1.1	0.119
Cs	AI009657	Citrate synthase	1.2	0.020*
Cs	H33235	Citrate synthase	1.3	0.013*
Dpyd	NM_031027	Dihydropyrimidine dehydrogenase	0.2	0.106[a]
Dpys	NM_031705	Dihydropyrimidinase	0.0	0.377[a]
Eno1	NM_012554	Enolase 1 (alpha)	3.7	0.000*
Eno2	AF019973	Enolase 2 (gamma), neuronal	5.9	0.000*
Eno3	NM_012949	Enolase 3, beta, muscle	0.7	0.457
Fasn	NM_017332	Fatty acid synthase	0.8	0.433
Fasn	AI179334	Fatty acid synthase	2.1	0.000*
Fh1	NM_017005	Fumarate hydratase 1	0.9	0.355
Gapdh	AFFX_Rat_GAPDH_3	Glyceraldehyde-3-phosphate dehydrogenase	3.0	0.001*
Gapdh	AFFX_Rat_GAPDH_5	Glyceraldehyde-3-phosphate dehydrogenase	2.7	0.003*
Gapdh	AFFX_Rat_GAPDH_M	Glyceraldehyde-3-phosphate dehydrogenase	2.6	0.003
Gapdh /// Gapdh-ps2	NM_017008	Glyceraldehyde-3-phosphate dehydrogenase /// glyceraldehyde-3-phosphate dehydrogenase, pseudogene 2	4.0	0.001*
Gck	NM_012565	Glucokinase	0.3	0.152
Gda	AF245172	Guanine deaminase	3.8	0.001*
Got1	D00252	Glutamic-oxaloacetic transaminase 1, soluble (aspartate aminotransferase 1)	1.1	0.589
Got2	NM_013177	Glutamic-oxaloacetic transaminase 2, mitochondrial (aspartate aminotransferase 2)	2.1	0.002*
Got2 /// LOC297793 /// LOC314123	BI296539	Glutamic-oxaloacetic transaminase 2, mitochondrial (aspartate aminotransferase 2) /// similar to aspartate aminotransferase, mitochondrial precursor (transaminase A) (glutamate oxaloacetate transaminase 2) /// similar to aspartate aminotransferase, mitochondrial precursor (transaminase A) (glutamate oxaloacetate transaminase 2)	1.6	0.029*
Gpd1	NM_022215	Glycerol-3-phosphate dehydrogenase 1 (soluble)	1.3	0.737

Table IV. *Continued*

Gene symbol	Representative public ID	Gene title	Fold	*P*-value
Gpd1	BI277042	Glycerol-3-phosphate dehydrogenase 1 (soluble)	0.3	0.048*
Gpi	BI283882	Glucose phosphate isomerase	3.9	0.000*
Gpt	NM_031039	Glutamic-pyruvate transaminase (alanine aminotransferase)	0.1	0.009*
Hk1	NM_012734	Hexokinase 1	0.8	0.476
Hk1	AFFX_Rat_ Hexokinase_3	Hexokinase 1	2.4	0.056
Hk1	AFFX_Rat_ Hexokinase_5	Hexokinase 1	0.8	0.559
Hk1	AFFX_Rat_ Hexokinase_M	Hexokinase 1	0.7	0.319
Hk2	NM_012735	Hexokinase 2	1.3	0.366
Hk2	BI294137	Hexokinase 2	1.8	0.001*
Hprt1	M86443	Hypoxanthine phosphoribosyltransferase 1	1.3	0.047*
Idh2	AI172491	Isocitrate dehydrogenase 2 ($NADP^+$), mitochondrial	0.5	0.000*
Idh3a	NM_053638	Isocitrate dehydrogenase 3 (NAD^+) alpha	2.3	0.001*
Idh3B	AI171793	Isocitrate dehydrogenase 3 (NAD^+) beta	0.7	0.000*
Idh3g	BI277627	Isocitrate dehydrogenase 3 (NAD), gamma	0.6	0.001*
Ldha	NM_017025	Lactate dehydrogenase A	2.6	0.004*
Ldhb	AA848319	Lactate dehydrogenase B	2.3	0.005*
Ldhc	NM_017266	Lactate dehydrogenase C	0.4	0.334
Ldhd	AI145761	Lactate dehydrogenase D	0.7	0.380
Ldhd	AI501131	Lactate dehydrogenase D	0.4	0.051
Mdh1	NM_033235	Malate dehydrogenase 1, NAD (soluble)	0.6	0.003*
Mdh1	BG671530	Malate dehydrogenase 1, NAD (soluble)	0.6	0.004*
Mdh2	NM_031151	Malate dehydrogenase 2, NAD (mitochondrial)	0.6	0.009
Me1	M30596	Malic enzyme 1, NADP(+)-dependent, cytosolic	3.1	0.003*
Me1	NM_012600	Malic enzyme 1, NADP(+)-dependent, cytosolic	2.0	0.035*
Nt5c3	AI409146	5′-Nucleotidase, cytosolic III	0.8	0.151
Nt5c3l	BF412799	5′-Nucleotidase, cytosolic III like	0.9	0.360
Nt5e	NM_021576	5′-Nucleotidase, ecto	1.1	0.745
Nt5e	BI289470	5′-Nucleotidase, ecto	1.1	0.696
Nt5m	AA819763	5′,3′-Nucleotidase, mitochondrial	2.6	0.052
Ogdh	BI277513	Oxoglutarate (alpha-ketoglutarate) dehydrogenase (lipoamide)	1.3	0.004*
Ogdh	BE103050	Oxoglutarate (alpha-ketoglutarate) dehydrogenase (lipoamide)	1.0	0.968
Pc	NM_012744	Pyruvate carboxylase	0.4	0.016*
Pdha1	AI411413	Pyruvate dehydrogenase (lipoamide) alpha 1	0.7	0.005*
Pdha1	BF561717	Pyruvate dehydrogenase (lipoamide) alpha 1	0.5	0.006*
Pdha2	NM_053994	Pyruvate dehydrogenase (lipoamide) alpha 2	0.1	0.302
Pdhb	BM389223	Pyruvate dehydrogenase (lipoamide) beta	0.4	0.001*
Pfkl	NM_013190	Phosphofructokinase, liver	1.0	0.952
Pfkm	NM_031715	Phosphofructokinase, muscle	0.8	0.001*
Pfkm	AI071717	Phosphofructokinase, muscle	0.3	0.143
Pfkm	BI291434	Phosphofructokinase, muscle	0.4	0.165
Pfkp	BM389769	Phosphofructokinase, platelet	3.5	0.001*
Pgam1	NM_053290	Phosphoglycerate mutase 1 (brain)	1.8	0.004*
Pgam2	NM_017328	Phosphoglycerate mutase 2 (muscle)	0.7	0.287
Pgk1	NM_053291	Phosphoglycerate kinase 1	0.3	0.131
Pgk1	NM_053291	Phosphoglycerate kinase 1	3.4	0.005*
Pgk1	BI279760	Phosphoglycerate kinase 1	2.2	0.011*
Pklr	NM_012624	Pyruvate kinase, liver and RBC	0.1	0.207
Pklr	M17685	Pyruvate kinase, liver and RBC	0.3	0.273
Pkm2	NM_053297	Pyruvate kinase, muscle	7.7	0.001*
Sdha	NM_130428	Succinate dehydrogenase complex, subunit A, flavoprotein (Fp)	0.8	0.009*
Sdhb	AI172320	Succinate dehydrogenase complex, subunit B, iron sulfur (Ip)	0.9	0.099
Sdhc	AI009817	Succinate dehydrogenase complex, subunit C, integral membrane protein	0.7	0.001*
Sdhd	AI410703	Succinate dehydrogenase complex, subunit D, integral membrane protein	1.0	0.911
Sdhd	AI176608	Succinate dehydrogenase complex, subunit D, integral membrane protein	0.8	0.009*
Sucla2	BF412750	Succinate-CoA ligase, ADP-forming, beta subunit	0.9	0.680
Sucla2	H31112	Succinate-CoA ligase, ADP-forming, beta subunit	0.6	0.596
Sucla2	AA923982	Succinate-CoA ligase, ADP-forming, beta subunit	0.7	0.001*
Suclg1	NM_053752	Succinate-CoA ligase, alpha subunit	0.5	0.000*
Suclg2	AI237518	Succinate-CoA ligase, GDP-forming, beta subunit	0.4	0.000*
Tpi1	NM_022922	Triosephosphate isomerase 1	3.0	0.001*
Uox	M24396	Urate oxidase	0.1	0.221[a]

Table IV. *Continued*

Gene symbol	Representative public ID	Gene title	Fold	*P*-value
Upb1	NM_053845	Ureidopropionase, beta	0.1	0.387[a]
Upp1	BI292558	Uridine phosphorylase 1	9.8	0.000*
Xdh	NM_017154	Xanthine dehydrogenase	2.5	0.001*

Expression levels of mRNAs related to glycolysis, the TCA cycle, fatty acid synthesis, nucleotide metabolism and the arachidonic acid cascade are shown. Pancreatic tissues derived from PDAC rats ($n = 6$) and controls ($n = 4$) were analyzed. *P*-values were calculated using Student's *t*-test.
[a]Expression levels were too low to be analyzed accurately by microarray analysis.
*$P < 0.05$.

Discussion

Serum metabolites are ideal biomarkers of human disease as the collection of serum samples is relatively non-invasive and multiple samples can be obtained to monitor disease progression. However, since serum represents the effects of metabolism in multiple organs, it is difficult to assign a metabolic fingerprint to specific metabolic processes of disease. Despite this, metabolites that change in the serum and display a similar change in diseased tissue, such as a cancerous lesion, are potential biomarkers specific to the metabolic process of the disease.

In this study, sera and pancreatic tissues from four control and six PDAC rats were subjected to non-targeted and targeted GC-MS-based metabolomics. The PCA score plots of the non-targeted metabolomic data of both the serum and pancreatic tissue showed a clear separation between control and PDAC rats, indicating the presence of distinct metabolite profiles in the serum and pancreatic tissue of PDAC-bearing rats compared with control rats.

Palmitoleic acid, which contributed to the distinctive metabolic profiles of the samples from the PDAC-bearing and control rats, was significantly decreased in the serum. Palmitoleic acid is a monounsaturated fatty acid biosynthesized from palmitic acid. Since palmitoleic acid is also contained in the diet, the decreases in the serum and pancreatic tissue of PDAC-bearing rats could be due to decreased absorption from the intestine. However, the decrease in PDAC-bearing rat lesions was apparently more pronounced in pancreatic tissue than in the serum. If the decrease in palmitoleic acid in the pancreatic tissue was due to its decreased levels in the serum, then the decreases found in the serum and pancreatic tissue should be similar. Instead, palmitoleic acid was decreased by a factor of ~2 in the serum and by a factor of ~7 or more in pancreatic tissue: while the decrease in palmitoleic acid in the pancreatic tissue of PDAC-bearing animals was not statistically different from the controls, it is notable that the highest level of palmitoleic acid in the PDAC rats was 13.77 p.p.m., whereas the lowest level of palmitoleic acid in the control rats was 100.33 p.p.m., a 7-fold difference. This suggests that decreased palmitoleic acid in pancreatic tissue was most likely due to increased consumption of the fatty acid in the PDAC lesions and that the decrease of palmitoleic acid in the serum was likely caused by its decrease in pancreatic tissues. Therefore, palmitoleic acid in the serum is a candidate biomarker for PDAC diagnosis.

In addition to palmitoleic acid, two other metabolites showed decreases in both the serum and pancreatic tissue: Arachidonic acid and 2(1*H*)-pyrimidinone were decreased non-significantly in the serum and decreased significantly in pancreatic tissue samples. Interestingly, the decrease of arachidonic acid could have been mediated by the increased expression of Alox5ap in PDAC (see Figure 3B). Increased activation of Alox5 could be the cause of the decrease of linoleic acid and arachidonic acid in the pancreatic tissue of PDAC-bearing rats. However, further investigations are needed to ascertain whether decreased linoleic acid and arachidonic acid were due to aberrant arachidonic acid metabolism or decreased synthesis of fatty acids.

One of the hallmarks of cancer is an increase of *de novo* fatty acid synthesis (16). A wide variety of tumors and their precursor lesions undergo exacerbated *de novo* biosynthesis of fatty acids from citrate by lipogenic enzymes—Acly, acetyl-CoA carboxylase and Fasn—irrespective of the levels of circulating lipids (16). In our study, however, we detected a decrease in the levels of several fatty acids. Possibly, decreased Acly expression (see Figure 3A) may have caused the decreases seen in the fatty acids in the pancreatic tissue of PDAC-bearing rats.

Another hallmark of cancer is the 'Warburg effect' (14,15) and decreased glucose has been reported in the serum and cancerous tissues of oral, colon and stomach cancer patients (17,18) and increased lactate has been reported in the serum of pancreatic cancer patients (19). In the present study, transcriptional analysis of PDAC tissues also suggested activation of anaerobic glycolysis and suppression of the TCA cycle. However, neither decreased glucose nor increased lactate were observed in the serum or pancreatic tissue of PDAC-bearing rats. The lack of a 'Warburg effect' in PDAC-bearing rats was probably due to the fact that after ~2 weeks of development, the PDACs were not advanced enough to disrupt pancreatic function and glucose control.

A notable difference between palmitoleic acid and glucose and lactic acid is that there are metabolic pathways dedicated to the regulation of glucose and lactic acid levels, but not to palmitoleic acid levels. Consequently, the tumor-mediated fluctuations in glucose and lactic acid seen in patients with more advanced tumors (17–19) may be absent in patients (and animal models) with less advanced tumors. In contrast, fluctuations of unregulated metabolites, such as palmitoleic acid, may occur in patients (and animal models) with less advanced tumors, as seen in the present study.

The increase in nucleotide degradation products xanthine, uridine and beta-alanine coupled with increased expression of several enzymes involved in nucleotide degradation (see Figure 3C) suggests that accelerated nucleotide degradation is occurring in the PDAC lesions. This accelerated nucleotide degradation may be due to the increased turnover of nucleotides in the PDAC lesions, which results from the increased nucleic acid synthesis in proliferating cells in the lesions.

Chenodeoxycholic acid, a major constituent of bile acids, was increased in the serum of PDAC-bearing rats. Metabolomic profiling of plasma of pancreas cancer patients by Urayama *et al.* (20) also showed an elevation of the bile acids taurocholic acid and tauroursodeoxycholic acid.

Concluding remarks

In summary, metabolites in the serum and pancreatic tissue of control and PDAC-bearing K-*ras*^{G12V} transgenic rats were analyzed by non-targeted and targeted GC-MS and transcripts in the PDAC lesions were analyzed by microarray. GC-MS analysis indicated that the profiles of the metabolites in the serum and pancreatic tissue samples derived from control rats differed from those derived from PDAC-bearing rats. A metabolite identified as palmitoleic acid was significantly decreased in the serum of PDAC-bearing rats and this decrease was likely due to its decrease in pancreatic tissue. Two other interesting metabolites are linoleic acid and arachidonic acid. These metabolites were significantly decreased in the pancreases of PDAC-bearing rats, possibly due to Alox5ap-mediated upregulation of Aox5 activity. Whether these metabolites could be markers of more advanced pancreas cancer remains to be determined. Finally, integration of the results of the non-targeted GC-MS analysis and transcriptomic

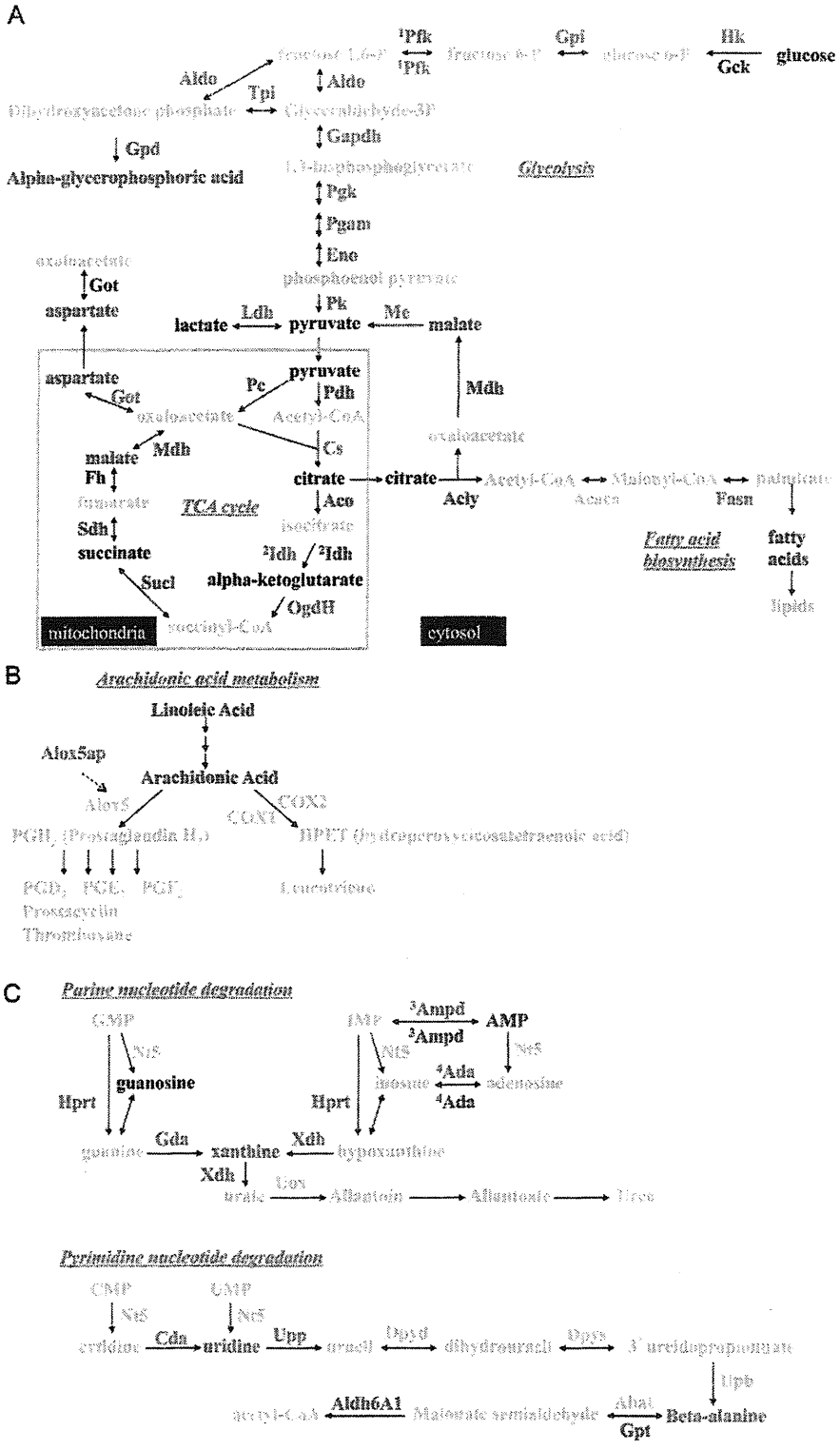

Fig. 3. Schematic representations of the most relevant metabolic and transcriptional differences in pancreatic tissues between PDAC and normal rats. Red, higher concentration in PDAC rats. Blue, lower concentration in PDAC rats. Black, not changed. Gray, not determined or unclear. [1]Pfkp was increased, whereas Pfkm was decreased. [2]Idh3a was increased, whereas Idh2, Idh3B and Idh3g were decreased. [3]Ampd3 was increased, whereas Ampd2 was decreased. [4]Ada, Adarb1 and Adarb2 were increased, whereas Adar was decreased.